Ongoing, long-term evolution of an unconformity that originated as a karstic surface in the Late Miocene: A case study from the Cayman Islands, British West Indies

Ting Liang*, Brian Jones

Department of Earth and Atmospheric Sciences, University of Alberta, Edmonton, Alberta, T6G 2E3, Canada

Corresponding author: E-mail address: tliang1@ualberta.ca *(T. Liang)*

ABSTRACT

On Grand Cayman and Cayman Brac, karst development on the upper surface of the Cayman Formation during the late Miocene lowstand produced the Cayman Unconformity. On Grand Cayman, this led to the development of a deep, atoll-shaped depression on the western part of the island. The ensuing Lower Pliocene transgression buried that unconformity and led to deposition of sediments that now form the Pedro Castle Formation. Today, on Grand Cayman, the dolostones of the Cayman Formation remain largely buried on the western half of Grand Cayman but are widely exposed on the central and eastern part of the island where they have been subjected to extensive weathering over the last 4.3 Ma. Although the situation is similar on Cayman Brac, uplift of the central core led to removal of the Pedro Castle Formation and much of the Cayman Formation. Karst development on both islands reflects the interplay between Neogene sea-level changes, climate, and tectonic uplift. Today, weathering is further modifying the Cayman Unconformity on the eastern parts of both islands.

The Cayman Unconformity on the central and eastern part of Grand Cayman is characterized by karst landforms, including a peripheral rim, sinkholes, solution-widened joints, and photolineaments (surface traces of joints and/or faults). The westward tilting of Cayman Brac (4.3 Ma to 400 ka) led to more severe weathering of the exposed Cayman Formation that included (1) enhancement of the peripheral rim and karst features on the upslope margin, and (2) higher denudation rates than on Grand Cayman. During the Messinian, the denudation rate on the west end of Grand Cayman was 0.03-0.10 mm yr^{-1}. In contrast, the denudation rate over the an estimated period of 4.9 to 6.2 Ma for the eastern half of Grand Cayman has been about 0.01 mm yr^{-1}, whereas on the east end of Cayman Brac it has been 0.03-0.04 mm yr^{-1}. On both

islands, substantial thicknesses of strata have been lost to erosion and the Cayman Unconformity has been subject to ongoing modification over a period of 4.9 to 6.2 Ma.

Keywords: karst topography; erosional unconformity; photolineaments; denudation rate; Cayman Islands

1. Introduction

The evolution of carbonate successions on isolated oceanic islands is fundamentally controlled by changes in sea level and tectonic activity (e.g., Schlanger and Premoli Silva, 1986; Lincoln and Schlanger, 1987; Jones and Hunter, 1994b). Weathering that takes place while the islands are subaerially exposed commonly leads to loss of strata and significant surface and subsurface modification of the exposed carbonates (Bathurst, 1975; Esteban and Klappa, 1983; James and Choquette, 1990; Flügel, 2004; Frisia and Borsato, 2010). Karst surfaces, which commonly develop under the influence of hot, humid climates, are particularly important because they (1) form the antecedent topography that may influence the early stages of sedimentation during the ensuing highstand (e.g., Purdy, 1974; Purdy and Winterer, 2001; Purkis et al., 2010; Liang and Jones, 2014), (2) will become the unconformities (i.e., sequence boundaries) that separate successive depositional packages (Tucker, 1990; Wright, 1994; Clari et al., 1995; Hillgärtner, 1998; Sattler et al., 2005), and (3) will delineate horizons with which meteoric diagenesis and/or dolomitization may be genetically related (Esteban and Klappa, 1983; James and Choquette, 1988; Tucker, 1990; Wright and Smart, 1994; Saller et al., 1994, 1999; Whitaker et al., 1999; Frisia and Borsato, 2010; Miller et al., 2012; Zhao and Jones, 2012). The karst topography that develops on erosional surfaces such as these is controlled by the complex interplay between numerous variables, including eustatic changes in sea level, tectonics, climate, hydrogeology, lithology, vegetation, porosity and permeability of the bedrock (White, 1988; Ford and Williams, 2007). The impact of factors such as sea-level change and tectonic movement are commonly difficult to decipher because they may produce the same end-result.

This study focuses on the unconformity that defines the upper boundary of the Cayman Formation (Miocene) that is found on Grand Cayman and Cayman Brac (Figs. 1, 2). This unconformity, named the Cayman Unconformity by Jones and Hunter (1994b), first developed during the Messinian lowstand. Estimates of eustatic fall at that time range from 30 m (Aharon et al., 1993) to 180 m (Pigram et al., 1992) below present-day sea level. Since then, this unconformity has experienced a complex developmental history. Today, parts of the original unconformity are still covered by younger sediments whereas other parts are exposed to the atmosphere and being actively weathered. Where exposed on the eastern part of Grand Cayman and the uplifted core of Cayman Brac, the surface of the Cayman Formation is characterized by phytokarst, pinnacles, sinkholes, and solution-widened joints (Doran, 1945; Folk et al., 1973; Jones and Smith, 1988; Squair, 1988; Jones, 1989, 1992). Although these islands have undergone different tectonic histories since deposition of sediments belonging to the Pedro Castle Formation ceased (Zhao and Jones, 2012, 2013; Liang and Jones, 2014), they are both free of surface streams and siliciclastic sediments.

This study focuses on the multistage evolution of the Cayman Unconformity by examining its geological evolution and the factors that have controlled its continued development in areas where it is now exposed on Grand Cayman and Cayman Brac. Comparison between the two islands allows an assessment of the influences that tectonic uplift as opposed to eustatic sea-level changes have had on the development of this unconformity. By doing so, this study demonstrates the complex developmental history that is responsible for the development of unconformities in carbonate successions on isolated oceanic islands.

2. Methods

Large areas in the interior of Grand Cayman and Cayman Brac are inaccessible because of the rugged karst terrain that is typically covered by dense tropical vegetation. Consequently, the karst forms exposed on the exposed surface of the Cayman Formation were delineated by using various techniques, including digital elevation models (DEMs), air photo interpretation and, where possible, field observations. The digital terrain data as supplied by the Lands and Survey Department of the Cayman Islands was used to generate the digital elevation models used in this study. The elevations were determined from LiDAR (Light Detection and Ranging) based on two laser returns per square meter with interpolation of the elevations based on a 3 x 3 m grid. The elevations for the bare ground, based on the return order and intensity of the laser signals, are considered accurate to ± 15 cm. ArcGIS 10 software was then used to produce three-dimensional (3D) geometrical views of the islands, including the areas that are largely inaccessible.

The "Hillshade" tool in ArcGIS 10 was used to create a shaded relief model of the surface by considering the illumination and shadows. As such, topographic highs, lows, open sinkholes, and photolineaments on the exposed Cayman Formation were highlighted by overlying the original DEMs onto the Hillshade map. In this study, elevation values along transect cutting across peripheral rims, ponds, embayment-shape depression and photolineaments were exported using ArcGIS functions. Then, these data were imported into Excel to obtain graphs of the profile, relative values of local relief and slope.

Open sinkholes, which may contain water, were defined by comparison between a depression-free DEM and the original DEM. The depression-free DEMs were generated automatically by the "Fill" tool in ArcGIS 10. Open sinkholes were identified by their sub-rounded to elliptical shape, their location on the exposed Cayman Formation, and that they are clearly not man-made. Sinkholes, solution-widened joints, and karst features smaller than 3 × 3 m could not be identified from the DEM because they are based on data with a minimum resolution of 3 × 3 m. Assessment of the small-scale features was restricted to examination of outcrops located along the coast because much of the interior of Grand Cayman and Cayman Brac is covered with dense tropical vegetation and is therefore largely inaccessible.

3. Terminology

Folk et al. (1973), based on exposures of the Cayman Formation at Hell on Grand Cayman, coined the term "phytokarst" as "a landform produced by rock solution in which boring plant filaments are the main agent of destruction". Phytokarst has a honeycomb appearance with gravitationally unoriented concavities (Folk et al., 1973; Jones, 1989), and surfaces that are covered by organic coatings that include fungi, sporangia, spores, mucilage, algae, and bacteria (Jones, 1989). Due to the organic-rich coatings, weathered phytokarst surfaces are grey to black and contrast sharply with the white dolostones of the Cayman Formation (Folk et al., 1973; Jones, 1989).

A sinkhole (= doline) is a closed depression, which originates through dissolution, collapse, and/or subsidence (Gams, 2003; Sauro, 2003; Ford and Williams, 2007). Sinkholes are typically circular to subcircular in plan form and can be up to ~1 km in diameter and several hundred metres deep (Sauro, 2003; Ford and Williams, 2007). Herein, the term sinkhole also includes "pit caves" as defined by Pace et al. (1993) and Mylroie and Carew (1995). Given that sinkholes may occur individually or in densely packed groups, the intensity (i.e., random, clustered, or regular) is used to define the distribution of sinkholes (Ford and Williams, 2007).

Joints are pull-apart breaks in consolidated rocks, with no displacement in any direction (Monroe, 1970; Ford and Williams, 2007). Commonly created by pressure release during erosion, they are prone to solution widening (e.g., Jones and Smith, 1988; Ford and Williams, 2007).

Photolineaments are narrow linear trends detectable on air photographs or satellite images that typically reflect the presence of closely spaced high-angle faults or fractures with little or no displacement (Ford and Williams, 2007; Sabins, 2007).

4. Geologic setting

Grand Cayman, Cayman Brac, and Little Cayman are located on the Cayman Ridge (Fig. 1). The Oriente Transform Fault (Fig. 1A), which forms the boundary between the Cayman Ridge and the Cayman Trench (up to 7686 m deep), also separates the Caribbean Plate from the North American Plate (Perfit and Heezen, 1978). This fault extends eastward from the north end of the Mid-Cayman Rise, which is an active spreading center located southwest of Grand Cayman. The Swan Island Transform Fault extends westward from the south end of Mid-Cayman Rise (MacDonald and Holcombe, 1978). Between the late Eocene and Oligocene, the Oriente Transform Fault detached the Cayman Islands from their parent arc and transported them to their present locations (Iturralde-Vinent, 1994; Calais and Mercier de Lépinay, 1995). Since the early Middle Miocene, localized extensional features began to form (Iturralde-Vinent and Macphee, 1999; Iturralde-Vinent, 2006). As a result, each of the Cayman Islands is now located on a different fault block (Matley, 1926; Horsfield, 1975; Stoddart, 1980; Liang and Jones, 2014).

Matley (1926) originally assigned the exposed Tertiary strata of the Cayman Islands to the Bluff Limestone, which was subsequently renamed as the Bluff Group by Jones et al. (1994a, 1994b). Unconformably overlain by the Pleistocene Ironshore Formation, the Bluff Group (Fig. 2) includes the unconformity-bounded Brac Formation, Cayman Formation, and Pedro Castle Formation (Jones et al., 1994a, 1994b). For the purposes of this paper, the critical aspects of this stratigraphic framework (Fig. 2) are:

- Deposition of sediments that now form the Cayman Formation took place during the Miocene (Jones, 1994; Jones et al., 1994a, b).
- Development of the Cayman Unconformity took place during the Messinian (Jones and Hunter, 1994b) between 7.246 to 5.333 Ma (dates from International Chronostratigraphic Chart – www.Stratigraphy.org/ICSchart/Chronodtrat2014-02.jpg) with most of the erosion probably taking place during the Messinian Salinity Crisis that lasted from 5.97 ± 0.2 Ma to 5.33 Ma (Krijgsman et al., 1999; Manzi et al., 2013; Pérez-Asensio et al., 2013). Accordingly, this phase of erosion lasted between 1.91 and 0.64 Ma.
- Deposition of the sediments that now forms the Pedro Castle Formation. This formation must be Pliocene because (1) it sits on the Cayman Unconformity that developed in the Messinian, and (2) *Stylophora*, which is common in this formation, became extinct in the Caribbean Sea at the end of the Pliocene (Frost, 1977). The average $^{87}Sr/^{86}Sr$ ratio for limestones and dolostones from the Pedro Castle Formation is 0.70905 (range of 0.70901 to 0.70910) for Grand Cayman (15 samples) and 0.70906 (range 0.70903 to 0.70910) for Cayman Brac (12 samples). According to the $^{87}Sr/^{86}Sr$ ratio curve of Farrell et al. (1995), this equates to an age of 2.0 to 4.4 Ma, whereas the modified curve of McArthur et al. (2006) yields an age of 4.3 to 4.4 Ma. This must be treated as a minimum age because many of the limestones in the Pedro Castle Formation have been partly to completely dolomitized. Thus, for the purposes of this study the Pedro Castle Formation is dated at between 5.33 (start of the Pliocene) and 4.3 Ma (minimum age from $^{87}Sr/^{86}Sr$ ratio) and therefore developed over a period of about 1 Ma (Fig. 2).
- The oldest part of the Ironshore Formation (Fig. 2) is estimated to be about 0.5 Ma (Vézina et al., 1999). The highest highstand position associated with this formation, 6 m above

present day sea level (asl), led to deposition of the sediments that now form Unit D (Vézina et al., 1999). The core of Cayman Brac remained above sea level during this highstand. On Grand Cayman it is possible that some parts of the interior of the eastern end of the island were inundated during this highstand for a short period of time.

5. The Cayman Unconformity

Based on present-day surface exposures, Grand Cayman can be divided into the western and eastern parts with the boundary being defined by the eastern boundary of the Ironshore Formation, which stretches from Cayman Kai along the eastern side of The Mountain and then to Breakers (Fig. 1B). Over most of the western half of the island, the Cayman Unconformity is buried beneath the Pedro Castle Formation and/or the Ironshore Formation apart from isolated outcrops like that at Hell. On the eastern part of the island, the Cayman Formation is widely exposed at the surface and being actively weathered. Relative to present day sea level, positive features on the Cayman Unconformity on Grand Cayman include the Mountain (22 m above sea level) and the peripheral ridges (up to 13.5 m asl) that are found along the south, east, and north coastlines (Fig. 3) on the eastern end of the island (Jones and Hunter, 1994b, their Fig. 12; Liang and Jones, 2014, their Fig. 14A). Negative features include (1) a deep depression (30 m below sea level) that is located under North Sound (Fig. 3) and (2) a sinkhole, now filled with the Pedro Castle Formation, located on the northeast corner of the island (QHW-1 – Fig. 1B) that had its base ~ 39 m below sea level (bsl). For the western part of the island, the Cayman Unconformity has a relief of at least 52 m. Although the relief on the eastern part of the island is up to 23 m (Fig. 4), the difference between the top of the Mountain and the base of the sinkhole at QHW-1 is 61 m.

Uplift of the east end of Cayman Brac means that the upper surface of the Cayman Formation has a maximum relief of 62 m (Fig. 5) and now dips westward at an angle of ~0.5° (Jones, 1994; Jones and Hunter, 1994a; Zhao and Jones, 2012, 2013; Liang and Jones, 2014). On the west end of the island, the Pedro Castle Formation sits on top of the unconformity. The exposed Cayman Unconformity on the uplifted core rises up to 46 m asl at the east end of the island. Peripheral rims are readily apparent on this weathered surface (Figs. 5, 6). Peripheral rims on the eastern upslope margin are more pronounced than those on the western downslope margin (Figs. 5, 6).

6. Cayman Unconformity buried by younger strata

On Grand Cayman and Cayman Brac, exposures that show the Cayman Unconformity overlain by younger strata are rare. In a quarry near Pedro Castle, the Cayman Unconformity, which dips at <1° to the northwest, is evident as a well-defined surface (~ 10 m asl in southeast corner of quarry) that is highlighted by the contrast in colour between the Cayman Formation and the overlying Pedro Castle Formation (Fig. 7A). The unconformity is generally smooth with no evidence of small-scale surface karst features. Penetrating into the dolostones from the unconformity are numerous sponge borings (Fig. 7B) and rare bivalve (*Lithophaga)* borings. In a small quarry located about 1 km southwest of the western end of the Georgetown airport runway, the Cayman Unconformity forms the quarry floor and is overlain by limestones of the Ironshore Formation (Fig. 7C). Although a relief of about 2 m is evident on the unconformity, the surface is generally smooth and devoid of small-scale karst features.

On Cayman Brac, the best exposures of the Cayman Unconformity are in a quarry that is located on the west end of the island (Fig. 7D). As in the Pedro Castle Quarry, the Cayman Unconformity is highlighted by the contrast in the colors of the dolostones that form the Cayman

Formation and the Pedro Castle Formation (Fig. 7E). There, the unconformity is characterized by small-scale variations in relief (Fig. 7E) and in some areas, sponge borings. No small-scale karst features are evident on the unconformity.

7. Cayman Unconformity exposed to the atmosphere

Exposed surfaces of the Cayman Formation (= Cayman Unconformity) on Grand Cayman and Cayman Brac are characterized by (1) various topographic features including peripheral rims, topographic highs and lows, (2) karst features that include sinkholes and honeycombed rock pinnacles, and (3) solution-widened joints and photolineaments (Doran, 1954; Folk et al., 1973; Rigby and Roberts, 1976; Stoddart, 1980; Jones and Smith, 1988; Squair, 1988; Jones, 1989, 1992, 1994; Jones and Hunter, 1994b; Liang and Jones, 2014).

7.1. Topographic features

7.1.1. Grand Cayman

Peripheral rims on Grand Cayman, which rise 8 to 13.5 m asl, are developed in the coastal areas of the eastern part of Grand Cayman (Figs. 4, 8). The landward limit of the peripheral rims, relative to the coastline, is constant (Jones and Hunter, 1994b; Liang and Jones, 2014). The peripheral rims are formed of dolostones that belong to the Cayman Formation. No evidence of the Pedro Castle Formation has been found on any of the rims.

Exposures in the interior of the island are characterized by a rugged surface that is mostly less than 3 m asl. Terrains with elevations > 3 m asl (Fig. 4) include the Mountain (up to 22 m asl), the area around High Rock Quarry (up to 9.3 m asl), and an inaccessible area between "The Mountain" and High Rock Quarry (up to 9.4 m asl).

In some of the coastal regions, there are large, brackish water ponds that are 0.4 to 1.2 m deep (Doran, 1954), and floored close to sea level. These shallow ponds, including Meagre Bay

Pond, Colliers Pond, and Malportas Pond, are irregular in shape (Figs. 4, 9). Meagre Bay Pond, located on the south shore close to Boddentown, ~ 1 km wide and 1 km long, is located behind a high beach barrier (Fig. 9B). This pond desiccates completely during periods of prolonged dry weather (Rigby and Roberts, 1976). Colliers Pond, located in the northeast part of the island, is 0.5 km wide and 1.5 km long, and located behind a beach sand barrier (Fig. 9C). During dry weather, the shallowest areas of Colliers Pond commonly desiccate (Rigby and Roberts, 1976). Malportas Pond, 2 km long and 0.7 km wide lies between a ridge formed of the Cayman Formation that stretches from North Side and Old Man Bay (up to 9.0 m asl), and "The Mountain" (Fig. 9D). The shallowest areas commonly desiccate during dry weather (Rigby and Roberts, 1976).

Embayment-shaped depressions, up to 1.8 km in diameter, are evident in the Guy Bay and Colliers areas on the east coast (Fig. 4). The bottom of these depressions are flat, with elevations being 1-2 m asl (Figs. 4, 9C). Their landward margins are topographic highs formed of the Cayman Formation, whereas their seaward margin varies. At Colliers, the embayment is separated from East Sound by Colliers Pond, which acts as a buffer zone between them. In contrast, the depression at Gun Bay is separated from East Sound by a peripheral rim.

7.1.2. Cayman Brac

On the uplifted core, peripheral rims that are up to 15 m higher than the surrounding land, are more pronounced than those on Grand Cayman (Figs. 6, 10). On the interior of the island, the elevation of the exposed Cayman Unconformity decreases gradually from east to west (Figs. 5, 6). Exposures on the upslope side are more rugged and have steeper slopes than those downslope (Figs. 5, 6, 10). The DEM reveals an elliptical depression near East End that is about 300 m long and 200 m wide (Fig. 6). This bowl-shaped depression, with a relief of up to 8 m, is developed behind the vertical cliff that defines the edge of the bluff in this area. It is morphologically similar to the ponds and the embayments found on Grand Cayman, suggesting that it may have originated in a similar manner prior to uplift of the island.

7.2. Karst features

On Grand Cayman and Cayman Brac, the exposed Cayman Formation is characterized by numerous sinkholes that are up to 10 m deep and 30 m in diameter (Doran, 1954; Folk et al., 1973; Jones and Smith, 1988; Jones, 1989, 1992; Liang and Jones, 2015). These sinkholes are open, filled with water, or filled with a variety of deposits that include rootcrete and various types of breccias that include limestone and dolostone lithoclasts held in white limestone matrices, or red or orange limestone matrices (Jones, 1992; Liang and Jones, 2015). Weathering of the dolostones between the sinkholes has produced honeycombed, sharp and jagged ridges and honeycombed, conical- or rectangular-shaped (up to 5 m high) pinnacles (Folk et al., 1973; Jones and Smith, 1988; Jones, 1989). The surfaces of the ridges and pinnacles and the walls of the sinkholes are dark grey to black in color (Fig. 11) due to the extensive phytokarst development (Folk et al., 1973; Jones and Smith, 1988; Squair, 1988; Jones, 1989).

7.2.1. Grand Cayman

Forty large sinkholes, up to 20 m in diameter and up to 0.7 m deep, have been recognized on the DEM (Fig. 4). Given that the sinkholes may be filled or partly filled by various deposits, the depths obtained from the DEM have to be treated as minimum estimates. Small sinkholes (< 3 m in diameter) cannot be recognized on the DEM because of resolution limits, and detailed mapping is impossible because the dense tropical vegetation and rugged surface produced by phytokarst mean that much of the island is inaccessible. On Grand Cayman, sinkholes identified on the DEMs are typically close to the photolineaments, especially in the area near "The Mountain" where photolineaments of Set I and Set II intersect (Fig. 4).

7.2.2. Cayman Brac

Fourteen large sinkholes, 6 to 25 m in diameter and up to 10 m deep, have been detected on the DEM that shows the surface topography of the exposed Cayman Formation on Cayman Brac (Fig. 6). Most of the sinkholes identified from the DEM are located on the eastern upslope areas of the interior part of the island (Fig. 6). The distribution, as revealed by the DEM, is biased because none of the small, deep sinkholes, with the diameter up to 1 m and the depth up to 20 m, can be detected on the DEM.

7.3. Joints and photolineaments

7.3.1. Grand Cayman

On Grand Cayman, three major joint sets that trend NNW-SSE, ENE-WSW, W-E are evident in areas where the Cayman Formation is well exposed (Rigby and Roberts, 1976; Jones, 1992; Fig. 4). Near Grape Tree Point, for example, two major sets trending at NNW-SSE and ENE-WSW are apparent (Fig. 4). In contrast, at Little Bluff, Breaker, and Old Issacs, the W-E and NNW-SSE sets dominate (Fig. 4). Vertical or westward dipping (~25°) solution-widened joints, up to 4 m wide (Fig. 12), in the Old Isaacs area, joints are open or filled with various deposits (Jones, 1992). There is no correlation between the orientation of the joints and their width (Jones, 1992). The vertical joints are commonly filled with flowstone and various types of breccia that are characterized by white dolostone lithoclasts held in white, red and orange limestone matrices, and dolostone matrices; whereas the westward dipping joints are commonly filled by caymanite (Jones and Smith, 1988; Jones, 1992).

Photolineaments are clearly visible on various air photographs and satellite images (e.g., Google World) that show the eastern part of Grand Cayman. Three sets of photolineaments, comprising Set I that trends N-S, Set II that trends ENE-WSW, and Set III that trends NNW-SSE, are evident in the areas around The Mountain and High Rock Quarry (HRQ). Around the Mountain, the N-S and ENE-WSW sets are more common than the NNW-SSE set (Fig. 4). Photolineaments in the areas around HRQ show similar trends to those in “The Mountain”, including the ENE-WSW set and the NNW-SSE set (Fig. 4). Photolineaments in the area between “The Mountain” and HRQ are dominated by the N-S set (Fig. 4). The bedrock in all of these areas is formed of the Cayman Formation. Attempts to locate these lineaments have, however, failed because the dense, tropical vegetation that covers these areas makes their recognition impossible. Transects across the photolineaments (sets I and II), derived from the DEM in the area around HRQ, show a series of ridges that are separated by valleys, with a local relief up to 2 m (Fig. 13). Each of the ridges appears symmetric, with gentle slopes (up to 5°) that merge with the valleys that are 20-100 m wide (Fig. 13).

The orientations of the photolineaments on Grand Cayman are similar to those of the joints. The NNW-SSE trending joints and NNW-SSE photolineaments (Set III) are parallel to the northeastern or eastern margin of the Grand Cayman block. The ENE-WSW trending joints present at Grape Tree Point, are comparable with the lineaments trending at ENE-WSW (Set II), which are parallel to the northeast trending faults that define the southeastern margin of Grand Cayman block of Grand Cayman (Figs. 1, 4). The E-W joints are consistent with the E-W faults that define the south and north margins of Grand Cayman block (Figs. 1, 4). The N-S photolineaments, in contrast, appear to be parallel to the eastern edge of the Grand Cayman block.

7.3.2. Cayman Brac

On Cayman Brac, the DEM shows that photolineaments are limited to the periphery of the uplifted core and dominated by three sets trending at ENE-WSW (Set IV in Fig. 6), E-W (Set V in Fig. 6), and WNW-ESE (Set VI in Fig. 6). Sets V and VI are only evident on the eastern half of the uplifted core.

Although the photolineaments in Set IV on Cayman Brac have a similar orientation to those in Set II on Grand Cayman, the orientations of the other photolineament sets on Cayman Brac and Grand Cayman differ. Transects across Set IV photolineaments, derived from the DEM, show that each photolineament is a ridge, which is separated from its neighbours by valleys that are up to 150 m wide (Figs. 6, 14D, 14F, 14H). Each of the ridges appears to be symmetric, with a gentle slope of 2-3° on each side (Figs. 14D, 14F, 14H). The relief of the photolineaments is variable, with the highest relief of up to 5 m being in the northeastern area (Figs. 6, 14D, 14F, 14H). Set V (E-W) photolineaments, with a relief up to 1.5 m, are only evident on the northeastern margin of the uplifted core (Figs. 6, 14E). A transect across this area shows that each photolineament is a ridge, with a relief up to 1.5 m, which is separated from its neighbours by valleys that are up to 12 m wide (Figs. 6, 14E). The ridges are symmetrical with slopes up to 3.5°. Set VI (WNW-ESE) photolineaments, evident only on the southeastern corner of the uplifted core, are less obvious on the DEM than the other two sets of photolineaments. Their relief (Set VI) between the ridges and surrounding valleys is typically lower than 1 m (Fig. 14G). On each side of the ridges, the slopes are < 2° (Fig. 14G). Valleys between these ridges are up to 15 m wide.

In general, the photolineaments are parallel to the faults that define the boundaries of the Cayman Brac fault block. The ENE-WSW (Set IV) photolineaments are parallel to the north and south margins of the Cayman Brac fault block (Figs. 1, 6). Set V, trending approximately E-W, is parallel to the escarpment between Spot Bay and East End, whereas the WNW-ESE trending set (Set VI) appears to parallel to the northeastern most limit of the Cayman Brac fault block (Figs. 1, 6).

8. Modifications of the exposed Cayman Unconformity

8.1. Topographic features

Based on laboratory experiments, Purdy (1974) suggested that the development of surface features on an exposed carbonate block depends on the balance between the rate of rainfall and the rate of the fluid flow off that block. In the "oversupply model", in which the former exceeds the later, a solution film will continuously cover the entire surface and a subdued surface will be produced. In the " balanced model", in which rainfall is slightly less than runoff, a solution meniscus will form over the interior part of the block. This leads to the formation of a continuous peripheral rim that surrounds a central solution depression that is characterized by a smooth floor. The "undersupply model", when the rate of rainfall is much lower than that of runoff, leads to a discontinuous solution film over the block and the formation of discontinuous peripheral rims and a rugged surface on the interior. According to these models, the peripheral rims that developed on the exposed surface of the Cayman Formation during the late Miocene probably formed when the rate of rainfall was less than that of the runoff (Jones and Hunter, 1994b; Liang and Jones, 2014).

The experiments done by Purdy (1974) used blocks of mature limestones that had had low porosity, low permeability, and devoid of fractures and/or joints. As a result, the simulated rainfall would have acted equally over the blocks because there were no internal heterogeneities that would have controlled the manner in which the water into and through the rock. In natural carbonate terrains, like those on the Cayman Islands, features such as fractures and joints commonly control water movement through the bedrock. That, in turn, may lead to heterogeneous patterns of dissolution that would strongly influence the development of surface landforms.

Uplift of Cayman Brac led to greater modification of the surface exposures of the Cayman Formation than on Grand Cayman. Based on his experiments, Purdy (1974) suggested that the peripheral rims on the surface of an inclined carbonate block would be intensified because surface runoff would be promoted in one direction and thereby lessen dissolution on the upslope edge of the block. This is applicable to Cayman Brac where the peripheral rim is more pronounced on the eastern upslope margin than on the western downslope margin. In addition, this unidirectional runoff also led to accentuation of the karst relief on the eastern upslope edge on Cayman Brac.

Embayment-shaped depressions found on the east coasts of Grand Cayman and Cayman Brac (Fig. 4) probably formed by wave activity. Their location on the eastern ends of the islands is consistent with the fact that those coasts experience the greatest fetch of any coast on the islands (Blanchon and Jones, 1995).

There are no surface streams or rivers on the Cayman Islands. Squair (1988) attributed the absence of surface rivers on Grand Cayman to (1) low relief, (2) small area (175 km^2), and/or (3) the high porosity and permeability of the bedrock. Observations indicate that the high porosity and permeability of the host carbonate is the most plausible explanation for the lack of surface water on Grand Cayman and Cayman Brac because any rain that falls on Grand Cayman and Cayman Brac quickly drains into the bedrock via joints, sinkholes and any other cracks that exist in the rock (Squair, 1988; Ng et al., 1992).

8.2. Sinkholes

On Grand Cayman, the DEM shows that large sinkholes (> 3 m in diameter) are commonly located close to the photolineaments. Such an association is expected given that sinkholes are commonly found in association with joints and fault systems that provide avenues for water movement and commonly focus dissolution in specific areas (Denizman and Randazzo, 2000; Faivre and Reiffsteck, 2002; Denizman, 2003; Florea, 2005; Gao et al., 2005; Basso et al., 2013).

Small-diameter sinkholes are common in all areas where the Cayman Formation is exposed and do not appear to be intimately linked to joints, photolineaments, or any other feature.

8.3. Joints and photolineaments

In many areas, like that on the southeast coast of Grand Cayman, joint development seems to have been an ongoing process. The presence of joints that are filled entirely with caymanite, which is a laminated, multicolored dolostone, indicates that the joints were formed and filled prior to dolomitization (Jones and Smith, 1988; Jones, 1992, his Fig. 5). In contrast, other joints that are filled by flowstone must have formed after the last phase of dolomitization. The open joints may have been formed more recently. Given the suggestion that joints on Grand Cayman are largely dictated by a regional tectonic control (Rigby and Roberts, 1976), the different timing of joints suggests the regional tectonic stresses along the margin of the Grand Cayman block are probably active periodically.

On Grand Cayman, the orientations of the photolineaments are generally similar to the joint directions that have been measured from outcrops (Rigby and Roberts, 1976; Ng et al., 1992). It is possible, therefore, that the photolineaments may be surface expressions of subsurface joints and/or faults that reflect a tectonic control (Ng et al., 1992). Regardless of their origin, the photolineaments probably represent subsurface features that are important elements of porosity and permeability and provide pathways for fluid movement (Ng, 1990; Ng et al., 1992). Indeed, Ng et al. (1992, their Fig. 11) suggested that the joints system might define the boundaries of the freshwater lens found on the eastern part of the island.

On Cayman Brac, the photolineaments have different orientations from those on Cayman Brac, probably because the tectonic stresses on that island were different from those on Grand Cayman (Ng et al., 1992). This is consistent with the fact that these two islands are located on different fault blocks. Furthermore, the photolineaments on Cayman Brac are most prominent on the eastern part of the island, suggesting that tectonic stresses on the eastern part of the Cayman Brac block were probably higher than those that affected the western part of the island. This is consistent with the fact that uplift was highest on the east end of Cayman Brac (Liang and Jones, 2014). On the uplifted core, identifiable photolineaments are limited to the periphery of the uplifted core. It is possible, however, that photolineaments in the interior of the uplifted core have been disguised by the development of other karst features.

9. Discussion

On the Cayman Islands, the Cayman Unconformity probably developed during the lowstand that triggered the Messinian Salinity Crisis. Although estimates for that eustatic fall range from 30 m (Aharon et al., 1993) to 180 m (Pigram et al., 1992) below present day sea level, the sea-level curve of Miller et al. (2005) indicates that it was generally < 40 m and Pérez-Asensio et al. (2013) argued that it was about 60 m below present day sea level.

On Grand Cayman, the lowest point yet found on the Cayman Unconformity (~ 39 m bsl) is in an old sinkhole on the northeast corner of the island that is now filled with the Pedro Castle Formation (Jones and Hunter, 1994b). On the western half of Grand Cayman the Cayman Unconformity is at least 30 m below sea level. These depths imply that sea level was 30 to 40 m below present day sea level when these landforms developed. Such depths are compatible with the sea level of Miller et al. (2005). This also implies that Grand Cayman has not undergone any vertical tectonic movement since the end of the Miocene.

The Cayman Unconformity on the west end of Grand Cayman and Cayman Brac is covered by the Pedro Castle Formation and/or the Ironshore Formation (Fig. 7). This buried unconformity provides a snapshot of the karst elements that existed prior to the sedimentation that took place following the Messinian lowstand. The most dominant topographic feature is an atoll-shape depression (Fig. 3), below North Sound, that has its base more than 30 bsl (Jones and Hunter, 1994b, their Fig. 12; Liang and Jones, 2014, their Fig. 14). On the western half of Grand Cayman, the peripheral rims that are found discontinuously along the southern, western and northern margins of the depression are now buried below younger strata. Available data show that the buried Cayman Unconformity typically dips from peripheral rims into the atoll-shaped depression with a slope of 0.6-1.4° (Jones and Hunter, 1994b; Wignall, 1995; Liang and Jones, 2014). The buried Cayman Unconformity is generally a smooth surface with minor topographic variations (Fig. 7B) that is locally characterized by bivalve and sponge borings (Wignall, 1995). The presence of these borings implies that the bedrock must have been hard and lithified before the Pliocene transgression. Some large sinkholes that are associated with the buried Cayman Unconformity (Jones, 1992) are filled with various combinations of caymanite, limestone, and dolomitized wakestones, packstones, and grainstones (Jones and Smith, 1988; Jones, 1992). The erosive processes associated with the transgression that followed the Messinian lowstand probably destroyed any small-scale surface karst features that once existed on the Cayman Unconformity (Wignall, 1995).

Today, the Cayman Formation exposed over most of the eastern half of Grand Cayman and much of the uplifted core on Cayman Brac is characterized by a highly weathered surface that typically has a desiccated, fretted, black, and honeycombed appearance (Fig. 11). The thickness of strata lost to erosion and the development of karst landforms on the upper surface of the Cayman Formation (Figs. 15, 16) reflect the interplay between eustatic sea level, tectonic movement, and the climatic conditions that existed during the lowstands.

The net loss of strata from the eastern part of Grand Cayman and the central part of Cayman Brac was the product of at least two phases of weathering: (1) Phase A that lasted for 0.64 to 1.91 Ma during the Messinian and predated deposition of the sediments that now form the Pedro Castle Formation, and (2) Phase B that lasted for ~ 4.3 Ma following the highstand that led to deposition of the sediments that now form the Pedro Castle Formation. Although highstands led to deposition of sediments that now form the Ironshore Formation, starting about 0.5 Ma, none of them were high enough to flood the elevated core of Cayman Brac. On Grand Cayman the 6 m highstand associated with Unit D of the Ironshore Formation may have led to short period of partial inundation over the interior of the eastern part of the island. Given that there is no physical evidence of deposition of the Ironshore Formation over the eastern part of Grand Cayman, this possibility is not included in the time estimate for the length of exposure since the deposition of the sediments that now form the Pedro Castle Formation ended. Erosion on the eastern part of Grand Cayman and on the core of Cayman Brac during phase B removed virtually all of the Pedro Castle Formation and the upper part of the Cayman Formation. The influence of climate on the development of karst landforms has been documented by many studies with rainfall commonly being deemed the key factor (e.g., Choquette and James, 1988; Smart and Whitaker, 1991; Wright, 1991; Saller et al., 1994; Ford and Williams, 2007). The topography of the Cayman Unconformity on Grand Cayman, for example, is lower on the western half than that on the eastern half of the island. This contrast in elevations is consistent with the fact that today, the highest rainfall is on the western part of Grand Cayman (Jones and Hunter, 1994b).

On Grand Cayman, a relief of at least 52 to 61 m developed on the surface of the Cayman Formation during the Messinian lowstand. Given that this erosion took place over a period of 0.64 to 1.91 Ma, the average denudation rate was 0.03-0.10 mm yr^{-1} on the western part of the island. Today, on the eastern part of the island, there is a maximum relief of 23 m on the exposed surface of the Cayman Formation, which is topographically higher than the Cayman Unconformity on the western part of the island. Although the cumulative length of time represented by weathering phases A (0.64 to 1.91 Ma) and B (4.3 Ma) is difficult to determine because of the oscillating sea levels that characterized the period that followed deposition of the Pedro Castle Formation, it is estimated to be a maximum of 4.9 to 6.2 Ma. The actual thickness of strata that was lost to erosion during this period is difficult to determine because the 23 m of relief now present on this part of the island may have been lost during phase A weathering, phase B weathering, or through both periods. If 23 m of strata were lost during the Messinian (phase A weathering), then that area would have then been covered by the Pedro Castle Formation, which is found to an elevation of 15 m asl around Pedro Castle Quarry. Today, however, no Pedro Castle Formation is found on the eastern part of Grand Cayman, other than the deposits that fill the old sinkhole at QHW-1 (Fig. 1B). Under this scenario, at least 38 m (23 m of Cayman Formation and 15 m of Pedro Castle Formation) have been lost to erosion. If 23 m of strata were lost during the Messinian, the average denudation rate would have been 0.01 to 0.04 mm yr^{-1}. If all of the weathering took place after deposition of the Pedro Castle Formation (phase B weathering), then the average denudation rate was 0.01 mm yr^{-1}. This range of values is lower than the values obtained for the weathering that took place on the western part of the island during phase A weathering.

The rate of subaerial erosion on a carbonate block can be enhanced by tectonic uplift because this increases the volume of the bedrock that is exposed above base level and commonly induces faults and fractures that serves as pathways by which aggressive solutions can penetrate the rock (Purdy and Waltham, 1999). This pattern is evident on Cayman Brac, where the eastern end of the island was tectonically uplifted at an average rate of 0.04-0.05 mm yr^{-1}, starting after deposition of the sediments that now form the Pedro Castle Formation ceased (Zhao and Jones, 2012, 2013; Liang and Jones, 2014), about 4.3 Ma. Phase B weathering began with the onset of uplift and available evidence indicates that the core of this island has remained above sea level since that time. On the Cayman Islands, the Cayman Formation is at least 165 m thick and the Pedro Castle Formation is at least 45 m thick (Jones, 1994; Jones et al., 1994b; Liang and Jones, 2014). On Cayman Brac, the Pedro Castle Formation has been stripped from most of the island, now being found only on the west end of the island where it is no more than 9 m thick. The thickness of the Cayman Formation increases from 20 m on the east end of the island to at least 100 m in the western part of the island (Jones, 1994; Jones et al., 1994b). Given that uplift was probably coincident with the onset of Phase B weathering, oscillating sea levels characterizing the period that followed deposition of the Pedro Castle Formation did not affect the uplifted core of Cayman Brac. Therefore, as much as 190 m of strata (145 m of Cayman Formation and 45 m of Pedro Castle Formation) may have been lost from the east end of Cayman Brac due to erosion that took place during weathering phases A and B over an estimated period of 4.9 to 6.2 Ma. This translates into an average denudation rate of 0.03-0.04 mm yr^{-1}. Determining the denudation rate during weathering Phase A as opposed to Phase B, however, is impossible because the amount of erosion that took place on the Cayman Formation during the Messinian lowstand cannot be determined.

The denudation rates calculated for erosion of the Cayman Formation and the Pedro Castle Formation on the Cayman Islands are generally less than the denudation rate of 0.07 to 0.14 mm yr^{-1} that Marshall and Davies (1984) determined for reef limestones in the southern part of the Great Barrier Reef and the rate of 0.11 to 0.69 mm yr^{-1} that Spencer (1985) derived for modern weathering of the reef limestones of the Ironshore Formation on Grand Cayman. This difference can probably be attributed to the fact that the reefal limestones, like those from the Pleistocene Ironshore Formation on Grand Cayman, are "softer" and more susceptible to weathering that the hard limestones and dolostones that characterize the Cayman Formation and Pedro Castle Formation.

On Grand Cayman and Cayman Brac, the buried Cayman Unconformity is found only on the western part of the islands, whereas the exposed Cayman Unconformity is found on the eastern and central parts of each island. This situation can be attributed to the following factors:

- The weathering rate during Phase A (Messinian lowstand) was probably higher on the western parts of each island, possibly due to higher rainfall in those areas, as it is today. This produced topographic lows that were subsequently filled-in during the next highstand and therefore became the sites where the maximum thicknesses of Pedro Castle Formation developed. As a result, the strata of this formation were not completely removed during the subsequent phases of subaerial erosion.
- Weathering during Phase B appears to have had the greatest impact on the strata of the Cayman Formation and Pedro Castle Formation that were exposed on the eastern parts of

these islands. For Cayman Brac, this can probably be attributed to the uplift that preferentially elevated the eastern end of the island. It is difficult, however, to assess the reason for this on Grand Cayman because there is no evidence pointing to the preferential uplift of the eastern end of that island.

Karst landforms can vary from locality to locality in accord with local climates, tectonic movement, and the nature of the substrates being weathered. In the Caribbean region, for example, Jamaica and Cuba have karst landscapes that are characterized by cockpit karst, cone karst, and tower karst (e.g., Pulina and Fagundo, 1992; Donovan, 2002), which are the norm in humid tropics. In contrast, Grand Cayman and Cayman Brac lack these large-scale, positive karst landforms. Purdy and Waltham (1999) argued that the development of large-scale, positive karst landforms was favoured by the uplift of strata with well-developed joint and fault systems that provide pathways for fluid penetration. This has, for example, lead to the development of large-scale karst landforms in many areas of the world (e.g., Brook and Ford, 1978; Waltham et al., 1983; Drogue and Bidaux, 1992; Ford and Williams, 2007), including the Guilin tower karst in China (Drogue and Bidaux, 1992; Purdy and Waltham, 1999) and Jamaican cockpit and conical hills (Sweeting, 1958). Although Grand Cayman and Cayman Brac are located on individual fault blocks, there is no evidence of faults that cut through the islands. The joint systems that are present in the Cayman Formation tend to be localized and irregularly distributed. Thus, the lack of large-scale karst features in the Cayman Formation can probably be attributed to the lack of faults and the poorly developed intersecting joint systems.

The development of an erosional unconformity in carbonate successions on isolated oceanic islands, such as Grand Cayman and Cayman Brac, is dictated by numerous variables, including eustatic sea-level changes, climatic conditions and tectonic movement. Uplift, in particular, may influence the development of the karst landforms by increasing the magnitude of base-level lowering, and controlling the runoff direction (Williams, 1972; Purdy and Waltham, 1999). Although the impact of uplift as opposed to eustatic sea-level changes on the development of erosional unconformity is commonly difficult to establish, the contrasts between the Cayman Unconformity on Grand Cayman and Cayman Brac show that uplift plays an important role. In general, uplift leads to accentuation of the topographic features and increased rates of erosion.

10. Conclusions

The upper surface of the Cayman Formation is an erosional unconformity that has developed through numerous phases of weathering between the late Miocene and the present day. Detailed comparison of the Cayman Unconformity on Grand Cayman and Cayman Brac has led to the following important conclusions, which are also applicable to processes that have affected carbonate successions on isolated islands throughout the world.

- The karst topography on an erosional unconformity is commonly characterized by peripheral rims, atoll-shape depressions and topographic highs, sinkholes and pinnacles, and solution-widened joints and photolineaments.
- Development of karst topography on an erosional unconformity on isolated carbonate islands reflects the interplay between eustatic sea-level changes, climate, and tectonic movements.
- The denudation rate on relatively flat landscapes is controlled largely by rainfall patterns. During the Messinian, the denudation rate of 0.03-0.10 mm yr^{-1} on the western part of Grand Cayman was much higher than that on the eastern part of this island. This

- difference is attributed to rainfall being highest on the western part of the island, as it is today.
- Tectonic uplift enhances the denudation rate on an erosional unconformity. The denudation rate on the east end of Cayman Brac over a period of 4.9 to 6.2 Ma was 0.03-0.04 mm yr^{-1}, which was more rapid than that on the eastern half of Grand Cayman where it was about 0.01 mm yr^{-1}.
- Photolineaments might be the surface expression of faults and/or joints, which are dictated by the region stress along the margin of fault-isolated block.

The conclusions derived from the carbonate successions on Grand Cayman and Cayman Brac are applicable to other isolated oceanic islands found throughout the world. Critically, it has shown that (1) thick successions of strata can be lost to erosion as karst processes are focused on the exposed carbonates, (2) the unconformities can develop through multiple phases of erosion, and (3) the same unconformity, despite developing on a small island, can represent significantly different lengths of exposure. The processes that control the development of unconformities in these settings commonly lead to the loss of significant thicknesses of bedrock and greatly impact the stratigraphic architecture of the successions.

Acknowledgments

We are grateful to the Natural Sciences and Engineering Research Council of Canada, which funded this research (Grant A6090 to Jones); Hendrik van Genderen from The Water Authority of Cayman Islands, who provided logistical support and assisted in the acquisition of data during the course of this study; The Lands and Survey Department, Cayman Islands who provided the data from which the digital elevation models for Grand Cayman and Cayman Brac were derived; and Valery Companiytsev, who provided technical support for ArcGIS 10. We are greatly indebted to Dr. Malcolm Wallace, an anonymous journal reviewer, and Editor Jasper Knight who provided constructive criticisms of an earlier version of this manuscript.

References

Aharon, P., Goldstein, L.S., Wheeler, C.W., Jacobson, G., 1993. Sea-level events in the South Pacific linked with Messinian salinity crisis. Geology 21, 771-775.

Basso, A., Bruno, E., Parise, M., Pepe, M., 2013. Morphometric analysis of sinkholes in a karst coastal area of southern Apulia (Italy). Environmental Earth Sciences 70, 2545-2559.

Bathurst, R.G.C., 1975. Carbonate Sediments and Their Diagenesis 12. Elsevier Science Publishing Company, Amsterdam, 658 pp.

Blanchon, P., Jones, B., 1995. Marine-planation terraces on the shelf around Grand Cayman: a result of stepped Holocene sea-level rise. Journal of Coastal Research 11, 1-33.

Brook, G.A., Ford, D.C., 1978. The origin of labyrinth and tower karst and the climatic conditions necessary for their development. Nature 275, 493-496.

Choquette, P.W., James, N.P., 1988. Introduction. In: James, N.P., Choquette, P.W. (Eds.), Paleokarst. Springer-Verlag, Berlin, Germany, pp. 1-21.

Clari, P.A., Dela Pierre, F., Martire, L., 1995. Discontinuities in carbonate successions; identification, interpretation and classification of some Italian examples. Sedimentary Geology 100, 97-121.

Denizman, C., 2003. Morphometric and spatial distribution parameters of karstic depressions, lower Suwannee River Basin, Florida. Journal Cave and Karst Studies 65, 29-35.

Denizman C., Randazzo A., 2000. Post-Miocene subtropical karst evolution, lower Suwannee River Basin, Florida. Geological Society of America Bulletin 112, 1804-1813.

Donovan, S.K., 2002. A karst of thousands: Jamaica’s limestone scenery. Geology Today 18, 143-151.

Doran, E., 1954. Landforms of Grand Cayman, British West Indies. Texas Journal of Science 6, 360-377.

Drogue, C., Bidaux, P., 1992. Structural and hydrogeological origin of tower karst in southern China (Lijiang plain in the Guilin region). Zeitschrift für Geomorphologie Neue Folge, Supplement-Band 36, 25-36.

Esteban, M., Klappa, C.F., 1983. Subaerial exposure environment. In: Scholle, P.A., Bebout, D.G., Moore, C.H. (Eds.), Carbonate Depositional Environments. American Association of Petroleum Geologists Memoir 33. American Association of Petroleum Geologists, Tulsa, United States, pp. 1-54.

Faivre, S., Reiffsteck, P., 2002. From doline distribution to tectonic movements: example of the Velebit mountain range, Croatia. Acta Carsologica 31, 139-154.

Farrell, J.W., Clemens, S.C., Gromet, L.P., 1995. Improved chronostratigraphy reference curve of late Neogene seawater $^{87}Sr/^{86}Sr$. Geology 23, 403-406.

Florea, L., 2005. Using state-wide GIS data to identify the coincidence between sinkholes and geologic structure. Journal of Cave Karst Studies 67, 120-124.

Flügel, E., 2004. Microfacies of Carbonate Rocks: Analysis, Interpretation and Application. Springer-Verlag, Berlin, 976 pp.

Folk, R.L., Roberts, H.H., Moore, C.H., 1973. Black phytokarst from Hell, Cayman Islands, British West Indies. Geological Society of America Bulletin 84, 2351-2360.

Ford, D., Williams, P.W., 2007. Karst Hydrogeology and Geomorphology. John Wiley and Sons, Chichester, United Kingdom, 562 pp.

Frisia, S., Borsato, A., 2010. Karst. In: Alonso-Zarza, A.M., Tanner, L.H. (Eds.), Carbonates in Continental Settings: Facies, Environments and Processes: Developments in Sedimentology. Elsevier, Oxford, United Kingdom, pp. 269-318.

Frost, S.H., 1977. Cenozoic reef systems of the Caribbean – prospects for paleoecologic synthesis. American Association of Petroleum Geologists Studies in Geology 4, 93-109.

Gams, I., 2003. Kras v Sloveniji v prostoru in času. Založba ZRC, ZRC SAZU, Ljubljana, 516 pp.

Gao, Y., Alexander, E.C. Jr, Barnes, R.J., 2005. Karst database implementation in Minnesota: analysis of sinkhole distribution. Environmental Geology 47, 1083-1098.

Hillgärtner, H., 1998. Discontinuity surfaces on a shallow-marine carbonate platform (Berriasian, Valanginian, France and Switzerland). Journal of Sedimentary Research 68, 1093-1108.

Horsfield, W.T., 1975. Quaternary vertical movements in the Greater Antilles. Geological Society of America Bulletin 86, 933-938.

Iturralde-Vinent, M.A., 1994. Cuban geology: A new plate-tectonic synthesis. Journal of Petroleum Geology 17, 39-70.

Iturralde-Vinent, M.A., 2006. Meso-Cenozoic Caribbean paleogeography: implications for the historical biogeography of the region. International Geology Review 48, 791-827.

Iturralde-Vinent, M.A., Macphee, R.D.E., 1999. Paleogeography of the Caribbean region: implications for Cenozoic biogeography. Bulletin of the American Museum of Natural History 238, 1-95.

James, N.P., Choquette, P.W., 1988. Paleokarst. Springer-Verlag, New York, 416 pp.

James, N.P., Choquette, P.W., 1990. Limestones-the meteoric diagenetic environment. In: McIlreath, I.A., Morrow, D.W. (Eds.), Diagenesis. Geological Association of Canada, Ottawa, Canada, pp. 35-74.

Jiménez-Moreno, G., Pérez-Asensio, J.N., Larrasoaña, J.C., Aguirre, J., Civis, J., Rivas-Carballo, M.R., Valle-Hernández, M.F., González-Delgado, J.A., 2013. Vegetation, sea-level and climate changes during the Messinian salinity crisis. Geological Society of America Bulletin 125, 432-444.

Jones, B., 1989. The role of micro-organisms in phytokarst development on dolostones and limestones, Grand Cayman, British West Indies. Canadian Journal of Earth Sciences 26, 2204-2213.

Jones, B., 1992. Void-filling deposits in karst terrains of isolated oceanic islands: a case study from Tertiary carbonates of the Cayman Islands. Sedimentology 39, 857-876.

Jones, B., 1994. Geology of the Cayman Islands. In: Brunt, M.A., Davies, J.E. (Eds.), The Cayman Islands: Natural History and Biogeography. Kluwer, Dordrecht, The Netherlands, pp. 13-49.

Jones, B., Hunter, I.G., 1994a. Evolution of an isolated carbonate bank during Oligocene, Miocene and Pliocene times, Cayman Brac, British West Indies. Facies 30, 25-50.

Jones, B., Hunter, I.G., 1994b. Messinian (Late Miocene) karst on Grand Cayman, British Indies: an example of an erosional sequence boundary. Journal of Sedimentary Research 64, 531-541.

Jones, B., Hunter, I.G., Kyser, T.K., 1994a. Revised stratigraphic nomenclature for Teriary strata of the Cayman Islands, British West Indies. Caribbean Journal of Science 30, 53-68.

Jones, B., Hunter, I.G., Kyser, T.K., 1994b. Stratigraphy of the Bluff Formation (Miocene-Pliocene) and the newly defined Brac Formation (Oligocene), Cayman Brac, British West Indies. Caribbean Journal of Science 30, 30-51.

Jones, B., Smith, D.S., 1988. Open and filled karst features on the Cayman Islands: implications for the recognition of paleokarst. Canadian Journal of Earth Sciences 25, 1277-1291.

Krijgsman, W., Hilgen, F.J., Raffi, I., Sierro, F.J., Wilson, D.S., 1999. Chronology, causes and progression of the Messinian salinity crisis. Nature 400, 652-655.

Liang, T., Jones, B., 2014. Deciphering the impact of sea-level changes and tectonic movement on erosional sequence boundaries in carbonate successions: a case study from Tertiary strata on Grand Cayman and Cayman Brac, British West Indies. Sedimentary Geology 305, 17-34.

Liang, T. and Jones, B., 2015. Petrographic and geochemical features of sinkhole-filling deposits associated with an erosional unconformity on Grand Cayman. Sedimentary Geology 315, 64-82.

Lincoln, J.M., Schlanger, S.O., 1987. Miocene sea-level falls related to the geologic history of Midway Atoll. Geology 15, 454-457.

Marshall, J.F., Davies, P.J., 1984. Last interglacial reef growth beneath modern reefs in the southern Great Barrier Reef. Nature 307, 44-46.

MacDonald, K.C., Holcombe, T.L., 1978. Inversion of magnetic anomalies and sea-floor spreading in the Cayman Trough. Earth and Planetary Science Letters 40, 407-414.

Manzi, V., Gennari, R., Hilgen, F., Krijgsman, W., Lugli, S., Roveri, M., Sierro, F.J., 2013. Age refinement of the Messinian salinity crisis onset in the Mediterranean. Terra Nova 25, 315-322.

Matley, C.A., 1926. The geology of the Cayman Islands (British West Indies) and their relation to the Bartlett Trough. Quarterly Journal of the Geological Society of London 82, 352-387.

McArthur, J.M., Rio, D., Massari, F., Castradori, D., Bailey, T.R., Thirwall, M., Houghton, S, 2006. A revised Pliocene record for marine- $^{87}Sr/^{86}Sr$ used to date an interglacial event recorded in the Cockburn Island Fromation, Antarctica Peninsula. Palaeogeography, Palaeoclimatology, Palaeoecology 242, 126-136.

Miller, C.R., James, N.P., Bone, Y., 2012. Prolonged carbonate diagenesis under an evolving late Cenozoic climate: Nullarbor Plain, southern Australia. Sedimentary Geology 261-262, 33-49.

Miller, K.G., Kominz, M.A., Browning, J.V., Wright, J.D., Mountain, G.S., Katz, M.E., Sugarman, P.J., Cramer, B.S., Christie-Blick, N., Pekar, S.F., 2005. The Phanerozoic record of global sea-level change. Science 310, 1293-1298.

Monroe, W.H., 1970. A Glossary of Karst Terminology. Geological Survey Water-Supply Paper 1899-K. United States Geological Survey, Washington D.C., United States, 26 pp.

Mylroie, J.E., Carew, J.L., 1995. Karst development on carbonate islands. In: Budd, D.A., Saller, A.H., Harris, P.M. (Eds.), Unconformities and Porosity in Carbonate Strata. American Association of Petroleum Geologists Memoir 63. American Association of Petroleum Geologists, Tulsa, United States, pp. 55-76.

Ng, K.C., 1990. Diagenesis of the Oligocene-Miocene Bluff Formation of the Cayman Islands; a petrographic and hydrogeochemical approach. Unpublished Ph.D Thesis, University of Alberta, Canada, 98 pp.

Ng, K.C., Jones, B, Beswick, R, 1992. Hydrogeology of Grand Cayman, British West Indies; a karstic dolostone aquifer. Journal of Hydrology 134, 273-295.

Pace, M.C., Mylroie, J.E., Carew, J.L., 1993. Petrographic analysis of vertical dissolution features on San Salvador Island, Bahamas. In: White, B. (Ed.), Proceedings of the Sixth Symposium on the Geology of the Bahamas. Bahamian Field Station, San Salvador, Bahamas, pp. 109-123.

Pérez-Asensio, J., Aguirre, J., Jiménez-Moreno, G., Schmiedl, G., Civis, J., 2013. Glacioeustatic control on the origin and cessation of the Messinian. Global and Planetary Change 111, 1-8.

Perfit, M.R., Heezen, B.C., 1978. The geology and evolution of the Cayman Trench. Geological Society of America Bulletin 89, 1155-1174.

Pigram, C.J., Davies, P.J., Feary, D.A., Symonds, P.A., 1992. Absolute magnitude of the second-order middle to late Miocene sea level fall, Marion Platform, Northeast Australia. Geology 20, 858-862.

Pulina, M., Fagundo, J.R., 1992. Tropical karst and chemical denudation of western Cuba. Geographia Polonica 60, 195-216.

Purdy, E.G., 1974. Reef configurations: cause and effect. In: Laporte, L.F. (Ed.), Reefs in Time and Space. Society of Economic Paleontologists and Mineralogists Special Publication 18, pp. 9-76.

Purdy, E.G., Waltham, D., 1999. Reservoir implication of modern karst topography. American Association of Petroleum Geologists Bulletin 83, 1774-1794.

Purdy, E.G., Winterer, E.L., 2001. Origin of atoll lagoons. Geological Society of America Bulletin 113, 837-854.

Purkis, S.J., Rowlands, G.P., Riegl, B.M., Renaud, P.G., 2010. The paradox of tropical karst morphology in the coral reefs of the arid Middle East. Geology 38, 227-230.

Rigby, J.K., Roberts, H.H., 1976. Geology, reefs and marine communities of Grand Cayman, British West Indies. *In:* Roberts, J.K., Roberts, H.H. (Eds.), Grand Cayman: Geology, Sediments, and Marine Communities. Brigham Young University, Geology Studies, Special Publication 4, pp. 1-95.

Sabins, F.F., 2007. Remote Sensing: Principles and Interpretation (3d ed.). Waveland Press, Long Grove, United States, 512 pp.

Saller, A.H., Budd, D.A., Harris, P.M., 1994. Unconformities and porosity development in carbonate strata: ideas from a Hedberg Conference. American Association of Petroleum Geologists Bulletin 79, 857-872.

Saller, A.H., Dickson, J.A.D., Matsuda, F., 1999. Evolution and distribution of porosity associated with sub-aerial exposure in upper Palaeozoic platform limestones, West Texas. American Association of Petroleum Geologists Bulletin 83, 1835-1844.

Sattler, U., Immenhauser, A., Hillgärtner, H., Esteban,M., 2005. Characterization, lateral variability and lateral extent of discontinuity surfaces on a carbonate platform (Barremian to lower Aptian, Oman). Sedimentology 52, 339-361.

Sauro, U., 2003. Dolines and sinkholes: aspects of evolution and problems of classification. Acta Carsologica 32, 41-52.

Schlanger, S.O., Premoli Silva, I., 1986. Oligocene sea-level falls recorded in mid-Pacific atoll and archipelagic apron settings. Geology 14, 392-395.

Smart, P.L, Whitaker, F.F., 1991. Karst processes, hydrology and porosity evolution. In: Wright, V.P., Esteban, M, Smart, P.L. (Eds.), Paleokarsts and Paleokarstic Reservoirs. University of Reading, Postgraduate Research Institute for Sedimentology, Occasional Publication Series, 2, pp. 1-55.

Spencer, T., 1985. Weathering rates on a Caribbean reef limestone: Results and implications. Marine Geology 69, 195-201.

Squair, C.A., 1988. Surface karst on Grand Cayman Island, British West Indies. Unpublished M.Sc. Thesis, University of Alberta, Canada, 107 pp.

Stoddart, D.R., 1980. Geology and geomorphology of Little Cayman. Atoll Research Bulletin 241, 11-16.

Sweeting, M.M., 1958. The karstlands of Jamaica. Geographical Journal 124, 184-199.

Tucker, M.E., 1990. Diagenetic processes, products and environments. In: Tucker, M.E., Wright, V.P., Dickson, J.A.D. (Eds.), Carbonate Sedimentology. Blackwell Science Publisher, Oxford, United Kingdom, pp. 314-364.

Vézina, J.V., Jones, B., Ford, D.C., 1999. Sea-level highstands over the last 500,000 years: evidence from the Ironshore Formation on Grand Cayman, British West Indies. Journal of Sedimentary Research 69, 317-327.

Waltham, A.C., Smart P.L., Friederich, H., Eavis, A.J., Atkinson, T.C., 1983. The caves of Gunung Sewu, Java. Transactions of the British Cave Research Association 10, 55-96.

Whitaker, F., Smart, P., Hague, Y., Waltham, D., Bosence, D., 1999. Structure and function of a coupled two-dimensional diagenetic and sedimentological model of carbonate platform evolution. Society for Sedimentary Geology Special Publication 62, 337-355.

White, W.B., 1988. Geomorphology and hydrology of carbonate terrains. Oxford University Press, London, 464 pp.

Wignall, B.D., 1995. Sedimentology and diagenesis of the Cayman (Miocene) and Pedro Castle (Pliocene) Formations at Safe Haven, Grand Cayman, British West Indies. Unpublished M.Sc. Thesis, University of Alberta, Canada, 110 pp.

Williams, P.W., 1972. Morphometric analysis of polygonal karst in New Guinea. Geological Society of America Bulletin 83, 761-796.

Wright, V.P., 1991. Paleokarst: types, recognition, controls and association. In: Wright, V.P., Estehan, M, Smart, P.L. (Eds.), Paleokarsts and Paleokarstic Reservoirs. University of Reading, Postgraduate Research Institute for Sedimentology, Occasional Publication Series, 2, pp. 56-88.

Wright, V.P., 1994. Paleosols in shallow marine carbonate sequences. Earth-Science Reviews 35, 367-395.

Wright, V.P., Smart, P.L., 1994. Paleokarst (dissolution diagenesis): Its Occurrence and hydrocarbon exploration significance. *In:* Wolf, K.H., Chilingarian, G.V. (Eds.), Diagenesis IV-Developments in Sedimentology 51. Elsevier Science, Amsterdam, Netherlands, pp. 477-517.

Zhao, H.W., Jones, B., 2012. Origin of "Island Dolostones": a case study from the Cayman Formation (Miocene), Cayman Brac, British West Indies. Sedimentary Geology 243-244, 191-206.

Zhao, H.W., Jones, B., 2013. Distribution and interpretation of rare earth elements and yttrium in Cenozoic dolostones and limestones on Cayman Brac, British West Indies. Sedimentary Geology 284-285, 26-38.

Figure Captions

Fig. 1. (A) Location of Cayman Islands relative to the Mid-Cayman Rise, Cayman Trench, and Oriente Transform Fault (modified from Jones, 1994, and based on maps from Perfit and Heezen, 1978, MacDonald and Holcombe, 1978). (B) Surface geology on Grand Cayman (modified from Jones, 1994) and position of the shelf-edge scarp of Grand Cayman (modified from Blanchon and Jones, 1995). (C) Surface geology on Cayman Brac (modified from Jones, 1994) and position of the shelf-edge scarp (derived from Google Earth images).

Fig. 2. (A) Simplified sea level curve for the last 10 Ma based on data in Miller et al. (2005, Supplemental Table S1 with points plotted at 0.05 Ma intervals). Dates for the Messinian Salinity Crisis (MSC) onset and termination taken from Jiménez-Moreno et al. (2013). Dates for the periods and stages based on the International Chronostratigraphic Chart (www.stratigraphy.org/ICSchart/ChronostratChart2014-02.jpg). (B) Stratigraphic succession of the Cayman Islands (from Jones, 1994b). (C) Simplified sea level curve for 6.25 to 5.0 Ma, which includes the Messinian Salinity Crisis (MSC), based on data in Miller et al. (2005, Supplemental Table S1 with points plotted every 0.01 Ma).

Fig. 3. Topography on upper surface of the Cayman Formation on Grand Cayman (from Liang and Jones, 2014, their Fig. 14). Surface is interpolated by Surfer 10 software from digital elevation data, outcrops and well data.

Fig. 4. Karst landforms and topography on the eastern half of Grand Cayman based on digital elevation model. The rose diagrams for joint orientations are from Rigby and Roberts (1976, their Fig. 30).

Fig. 5. Topography on upper surface of the Cayman Formation on the uplifted core of Cayman Brac (from Liang and Jones, 2014, their Fig. 15). Surface is interpolated by Surfer 10 software from digital elevation data, outcrops and drilling wells.

Fig. 6. Karst landforms and topography on the Cayman Unconformity exposed on the uplifted core of Cayman Brac. Based on digital elevation model.

Fig. 7. Features of the Cayman Unconformity in outcrops where the Cayman Formation (CF) is overlain by the Pedro Castle Formation (PCF) or Ironshore Formation (IF). (A) South wall of Pedro Castle Quarry (Grand Cayman) showing the Cayman Unconformity (arrows) between the Cayman Formation and the Pedro Castle Formation. Quarry wall is about 12 m high, with the unconformity being about 10 m above sea level. (B) Close-up showing sponge borings extending down from Cayman Unconformity (arrows) and small cavities partly filled with internal sediments. Pedro Castle Quarry. (C) Limestones of the Ironshore Formation resting on top of irregular upper surface of the Cayman Formation (= Cayman Unconformity). Quarry southwest of west end of runway at Georgetown Airport. (D) General view of Cayman Unconformity (arrows) between the Cayman Formation and Pedro Castle Formation in quarry located at west end of Cayman Brac. Quarry wall is about 5 m high. (E) Minor relief on the Cayman Unconformity. Quarry at west end of Cayman Brac.

Fig. 8. DEM of eastern part of Grand Cayman (A) showing locations of topographic transects across the peripheral rims (B, C, D, E and F).

Fig. 9. DEM of eastern part of Grand Cayman (A) showing locations of topographic transects ponds (B, C, and D). Black squares indicate locations of Figure 13A and 13B.

Fig. 10. DEM of Cayman Brac (A) showing locations of topographic transects across peripheral rims (B, C, D, E and F) . Blue squares indicate locations of Figure 14A, 14B and 14C.

Fig. 11. Features commonly found on surface exposures of the Cayman Formation. (A) View of phytokarst at Hell, Grand Cayman showing jagged pinnacles around sinkholes and solution-widened joints that are filled with water and sediment. Pinnacles in foreground are up 1.5 m high. (B) Phytokarst developed in interior of Cayman Brac. Pinnacles in foreground are up to 2 m high. (C) Sinkhole that is about 1 m in diameter and at least 20 m deep developed in dolostones of the Cayman Formation, interior of Cayman Brac. (D) Solution-widened joint in dolostones of Cayman Formation, quarry at west end of Cayman Brac. Width of joint at water level is about 2 m.

Fig. 12. Solution-widened joint (~ 1 m wide) in dolostones of the Cayman Formation, Old Isaacs on Grand Cayman. The NNW-SSE joint is filled largely with dolostones lithoclasts that came from the Cayman Formation.

Fig. 13. DEM of selected areas (see Figure 9 for precise location) on eastern part of Grand Cayman (A, B) showing locations of topographic transects (C-C', D-D', E-E', F-F', and G-G') across the photolineaments.

Fig. 14. Topographic transects (D-D', E-E', F-F', G-G', H-H', and I-I') showing topography of the photolineaments on Cayman Brac. See Figure 10 for precise location. Note that the peripheral rims on the upslope margin are more pronounced than those on Grand Cayman.

Fig. 15. Oblique view of the exposed Cayman Unconformity on the eastern half of Grand Cayman that is still evolving today. Note photolineaments (red arrows) in the area between The Mountain and HRQ. Vertical exaggeration is 50, in order to illustrate the karst landforms.

Fig. 16. Oblique view of the exposed Cayman Unconformity on the uplifted core of Cayman Brac. Blue arrows indicate photolineaments. Vertical exaggeration is 50, in order to illustrate the karst landforms.

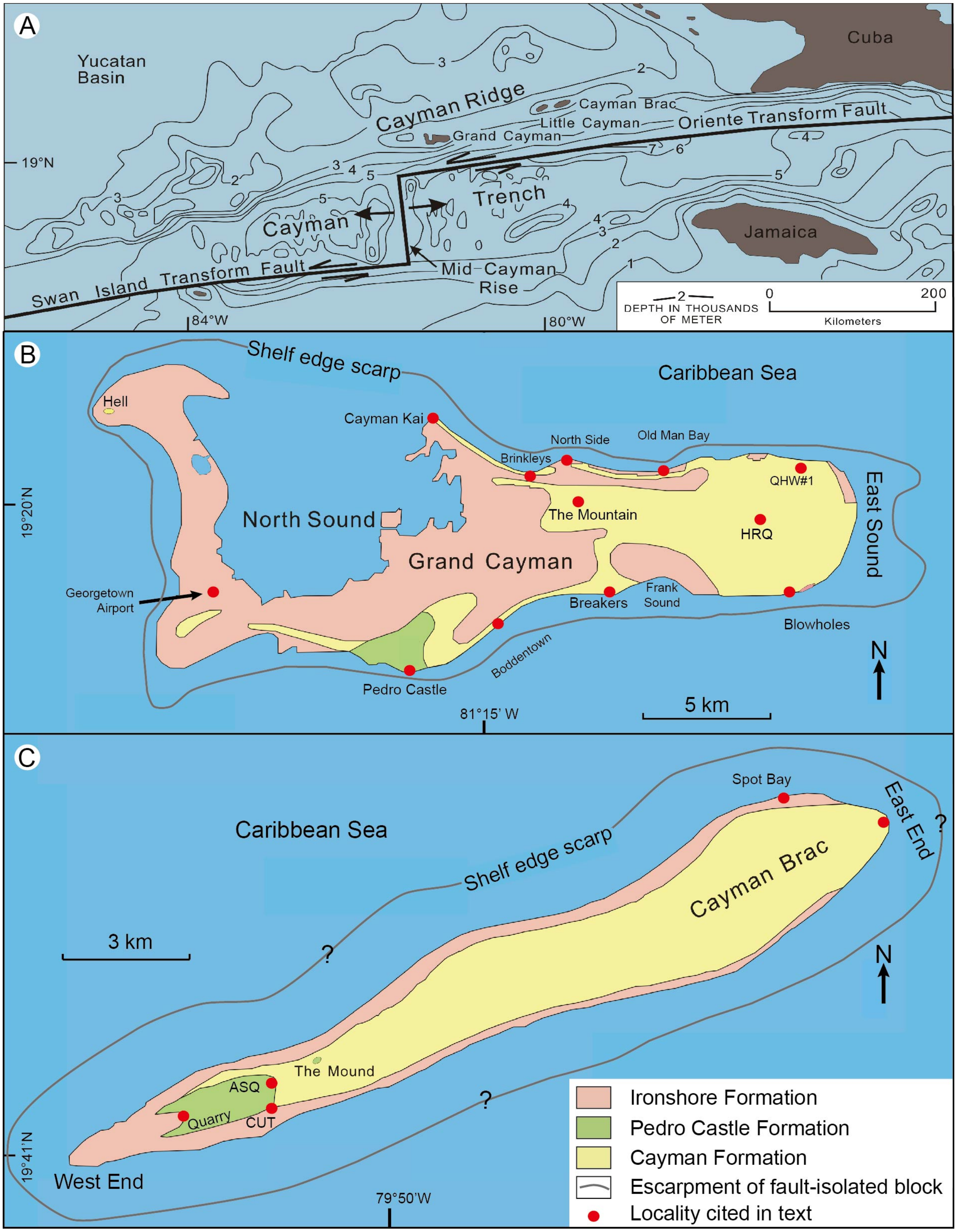
A
Yucatan Basin
Cuba
Cayman Ridge
Cayman Brac
Little Cayman
Grand Cayman
Oriente Transform Fault
19°N
Cayman
Trench
Jamaica
Swan Island Transform Fault
Mid-Cayman Rise
DEPTH IN THOUSANDS OF METER
0
200
Kilometers
84°W
80°W
B
Shelf edge scarp
Caribbean Sea
Hell
Cayman Kai
North Side
Old Man Bay
Brinkleys
QHW#1
East Sound
19°20'N
North Sound
The Mountain
HRQ
Grand Cayman
Georgetown Airport
Breakers
Frank Sound
Blowholes
Boddentown
Pedro Castle
81°15' W
5 km
N
C
Spot Bay
East End
Caribbean Sea
Shelf edge scarp
Cayman Brac
3 km
The Mound
ASQ
Quarry
CUT
19°41'N
West End
79°50'W
Ironshore Formation
Pedro Castle Formation
Cayman Formation
Escarpment of fault-isolated block
Locality cited in text

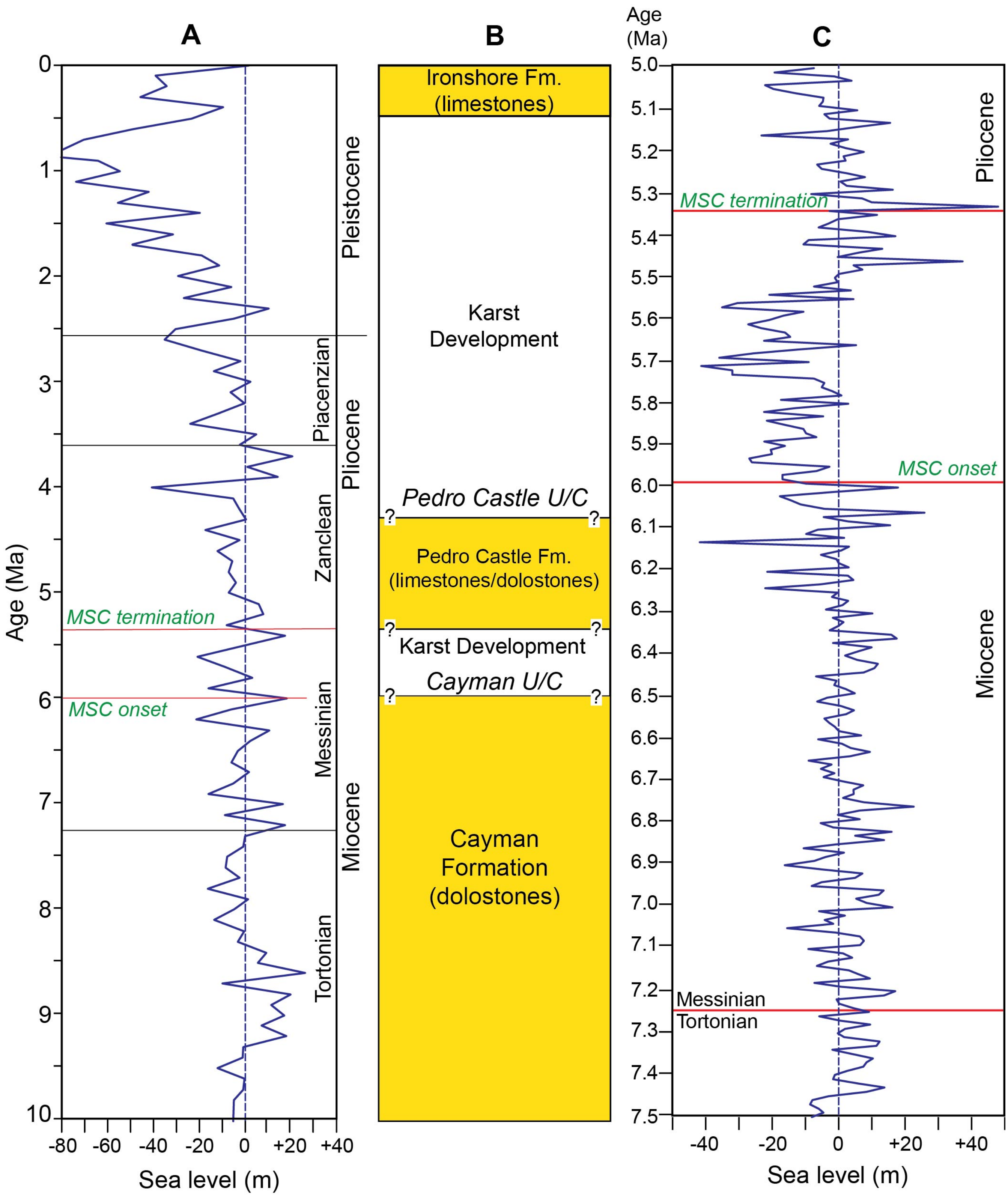
A
B
C
Age (Ma)
Sea level (m)
Pleistocene
Pliocene
Miocene
Piacenzian
Zanclean
Messinian
Tortonian
MSC termination
MSC onset
Ironshore Fm.
(limestones)
Karst
Development
Pedro Castle U/C
Pedro Castle Fm.
(limestones/dolostones)
Karst Development
Cayman U/C
Cayman
Formation
(dolostones)
Age
(Ma)
Messinian
Tortonian
Sea level (m)

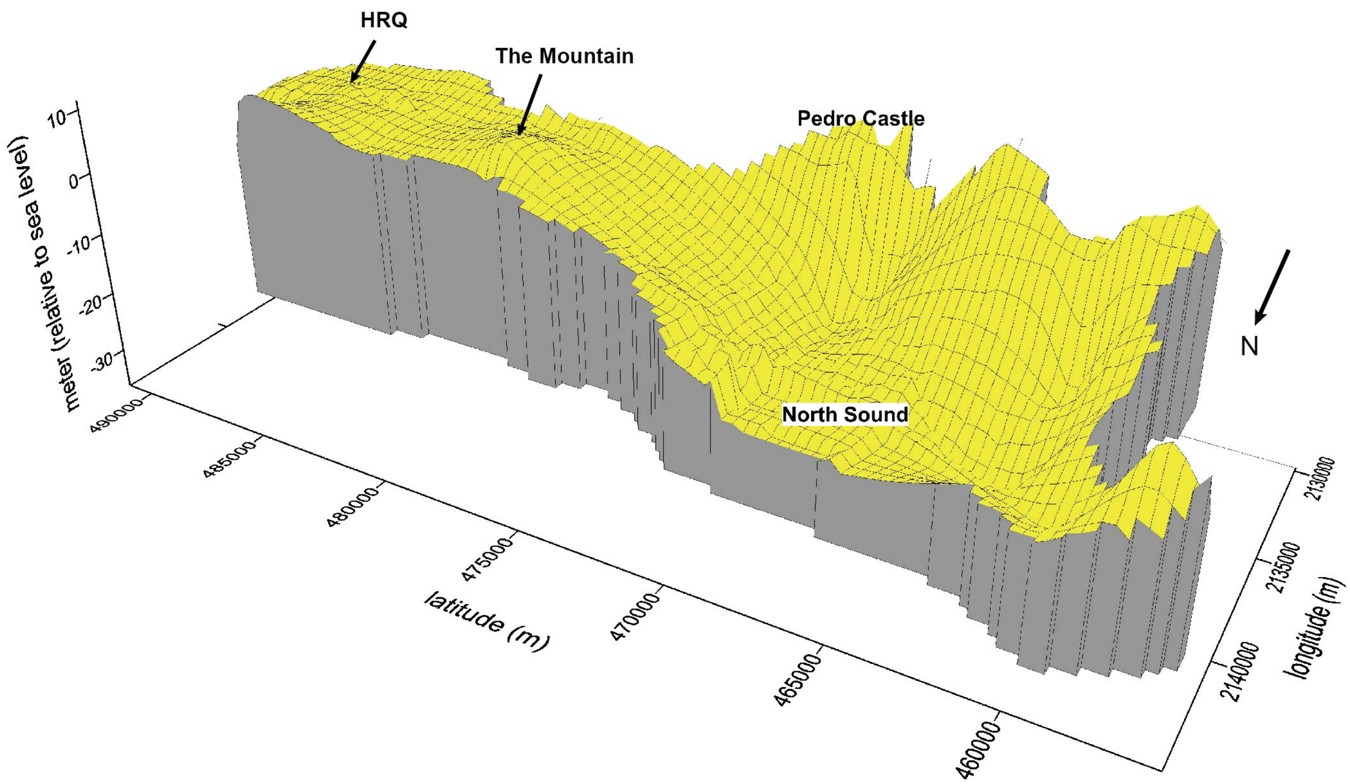
HRQ
The Mountain
Pedro Castle
North Sound
N
meter (relative to sea level)
10
0
-10
-20
-30
490000
485000
480000
475000
470000
465000
460000
latitude (m)
2130000
2135000
2140000
longitude (m)

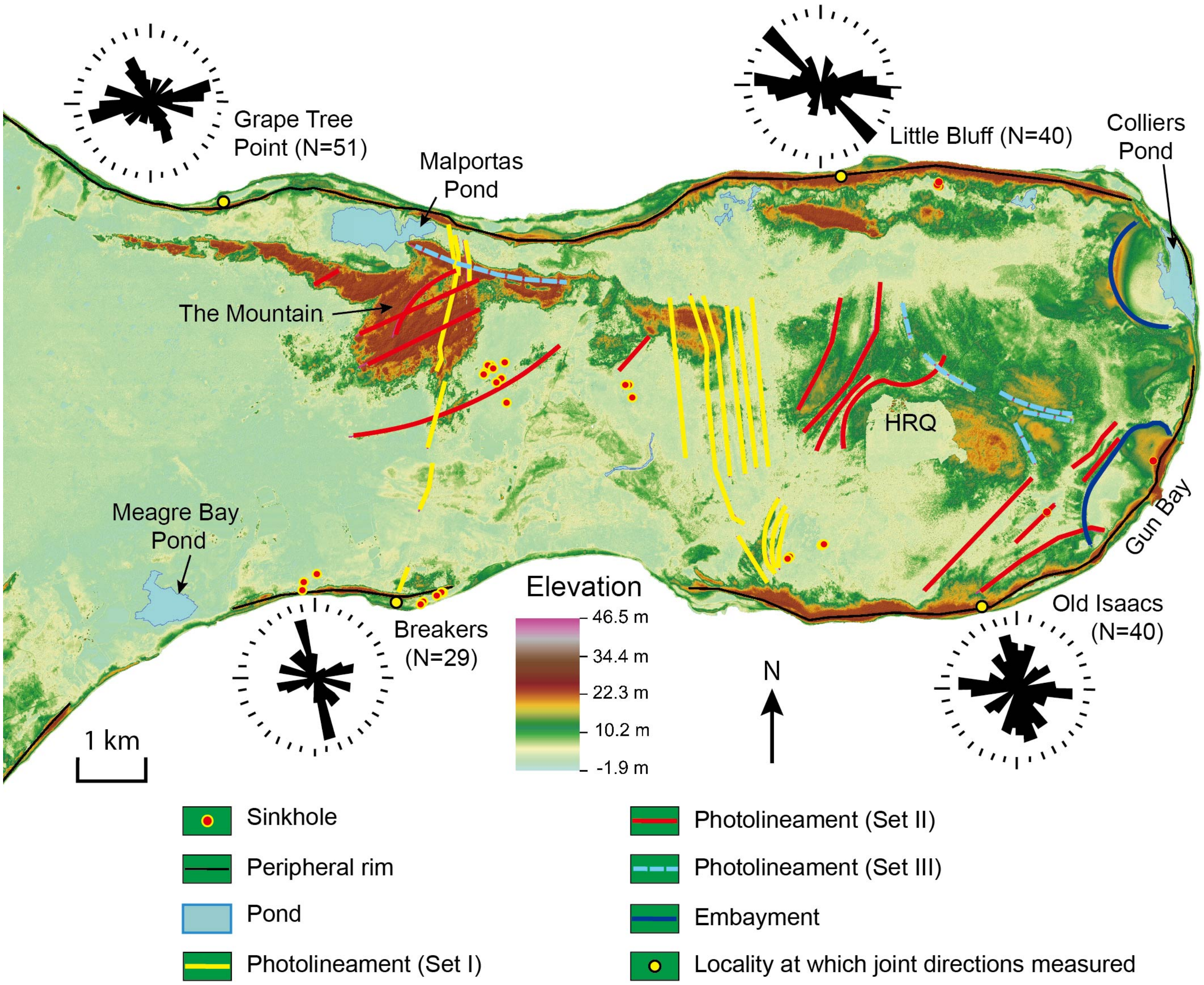

Grape Tree Point (N=51)
Malportas Pond
Little Bluff (N=40)
Colliers Pond
The Mountain
HRQ
Meagre Bay Pond
Gun Bay
Breakers (N=29)
Old Isaacs (N=40)
Elevation
46.5 m
34.4 m
22.3 m
10.2 m
-1.9 m
N
1 km
Sinkhole
Peripheral rim
Pond
Photolineament (Set I)
Photolineament (Set II)
Photolineament (Set III)
Embayment
Locality at which joint directions measured

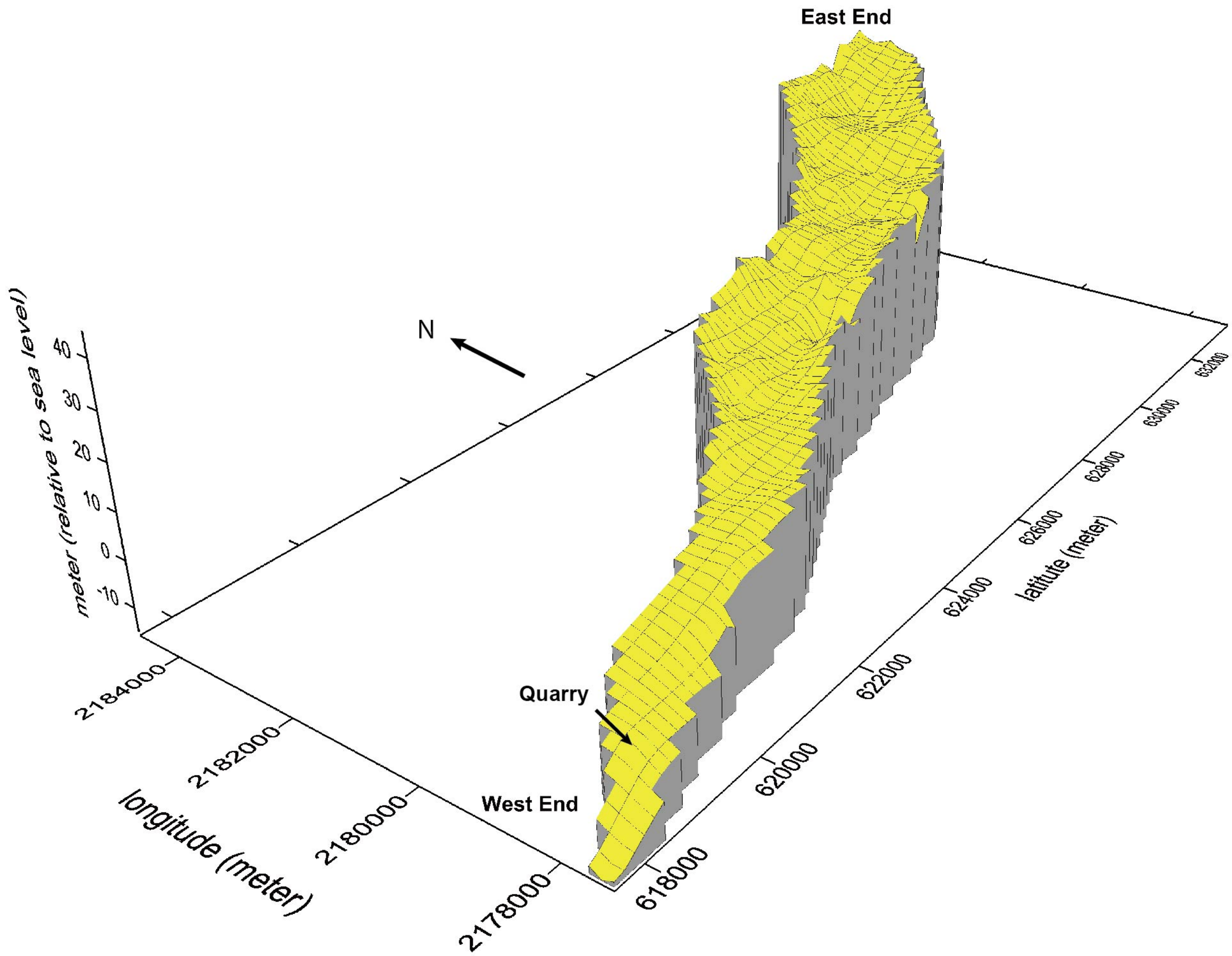
East End
N
meter (relative to sea level)
40
30
20
10
0
-10
Quarry
West End
2184000
2182000
2180000
2178000
longitude (meter)
618000
620000
622000
624000
626000
628000
630000
632000
latitute (meter)

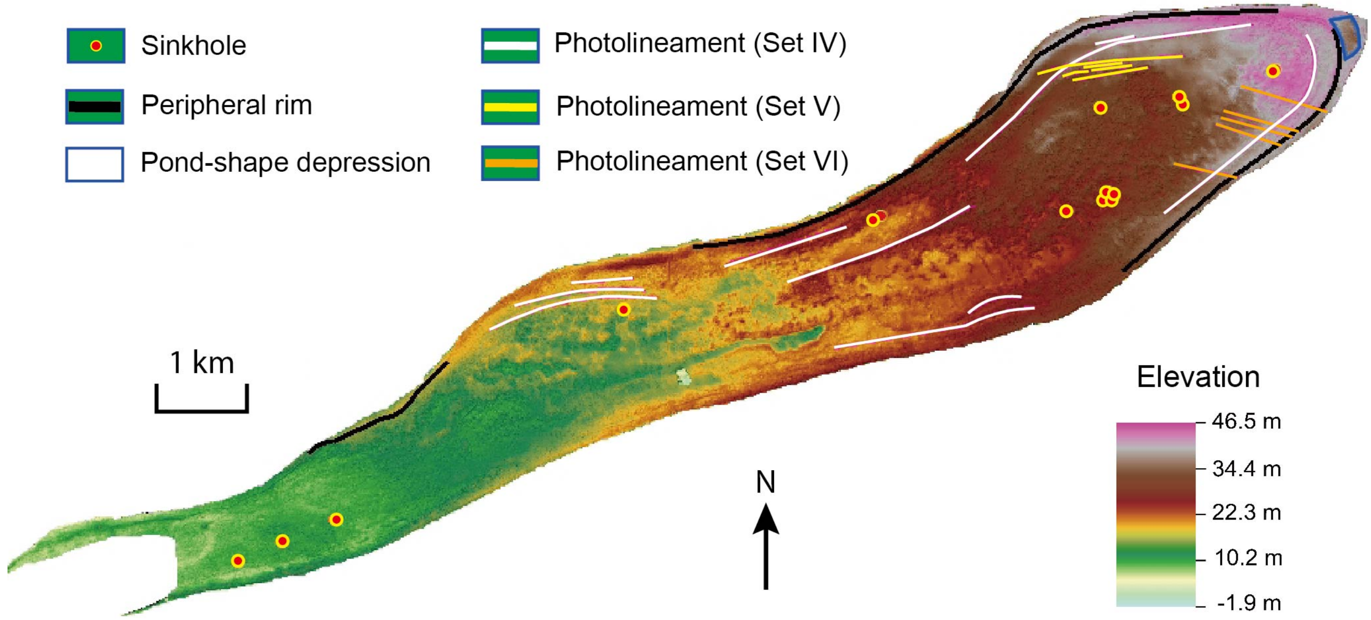
Sinkhole
Peripheral rim
Pond-shape depression
Photolineament (Set IV)
Photolineament (Set V)
Photolineament (Set VI)
1 km
N
Elevation
46.5 m
34.4 m
22.3 m
10.2 m
-1.9 m

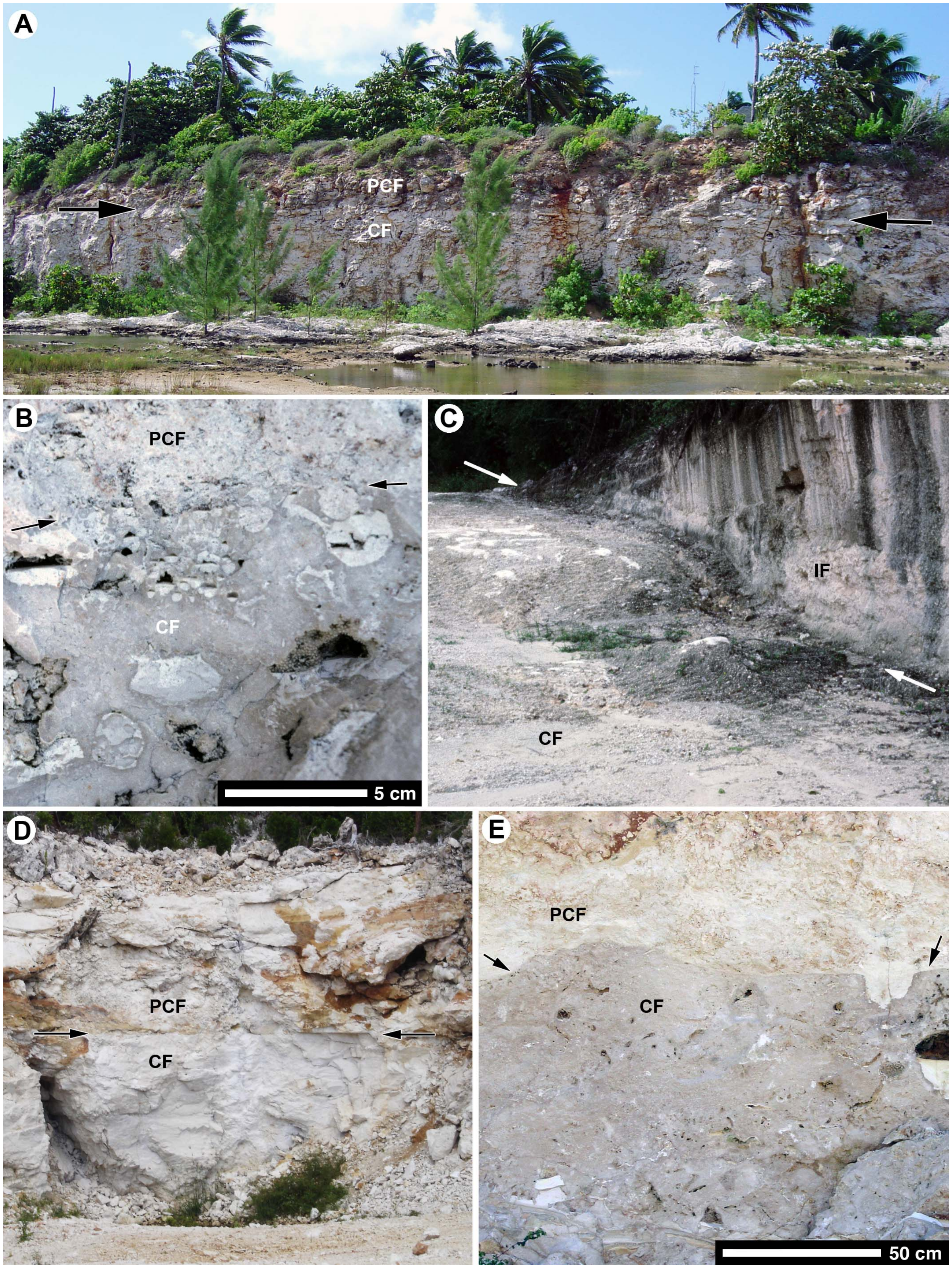
A
PCF
CF
B
PCF
CF
5 cm
C
IF
CF
D
PCF
CF
E
PCF
CF
50 cm

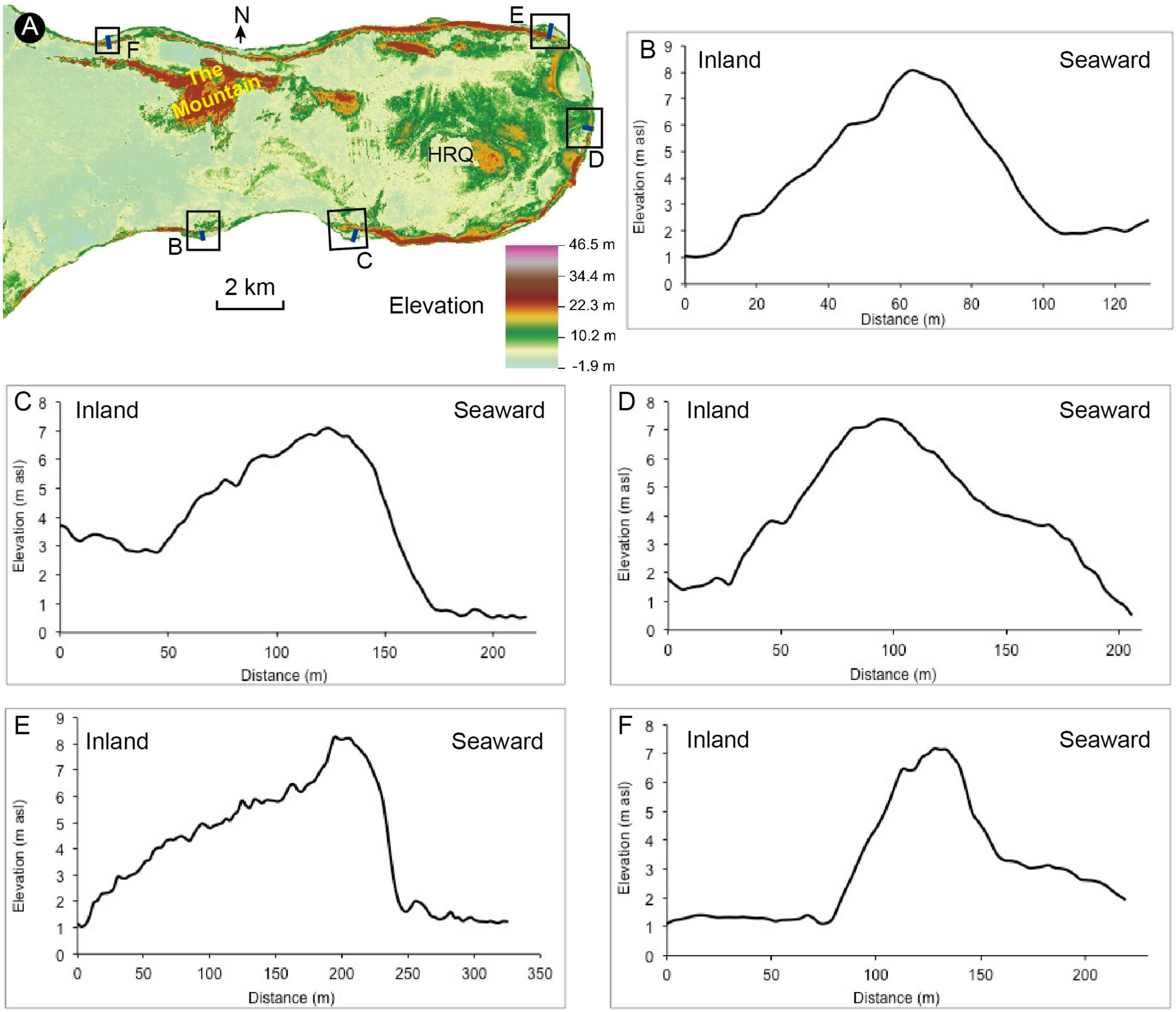
A
N
E
F
D
B
C
The Mountain
HRQ
2 km
Elevation
46.5 m
34.4 m
22.3 m
10.2 m
-1.9 m
Inland
Seaward
Elevation (m asl)
Distance (m)

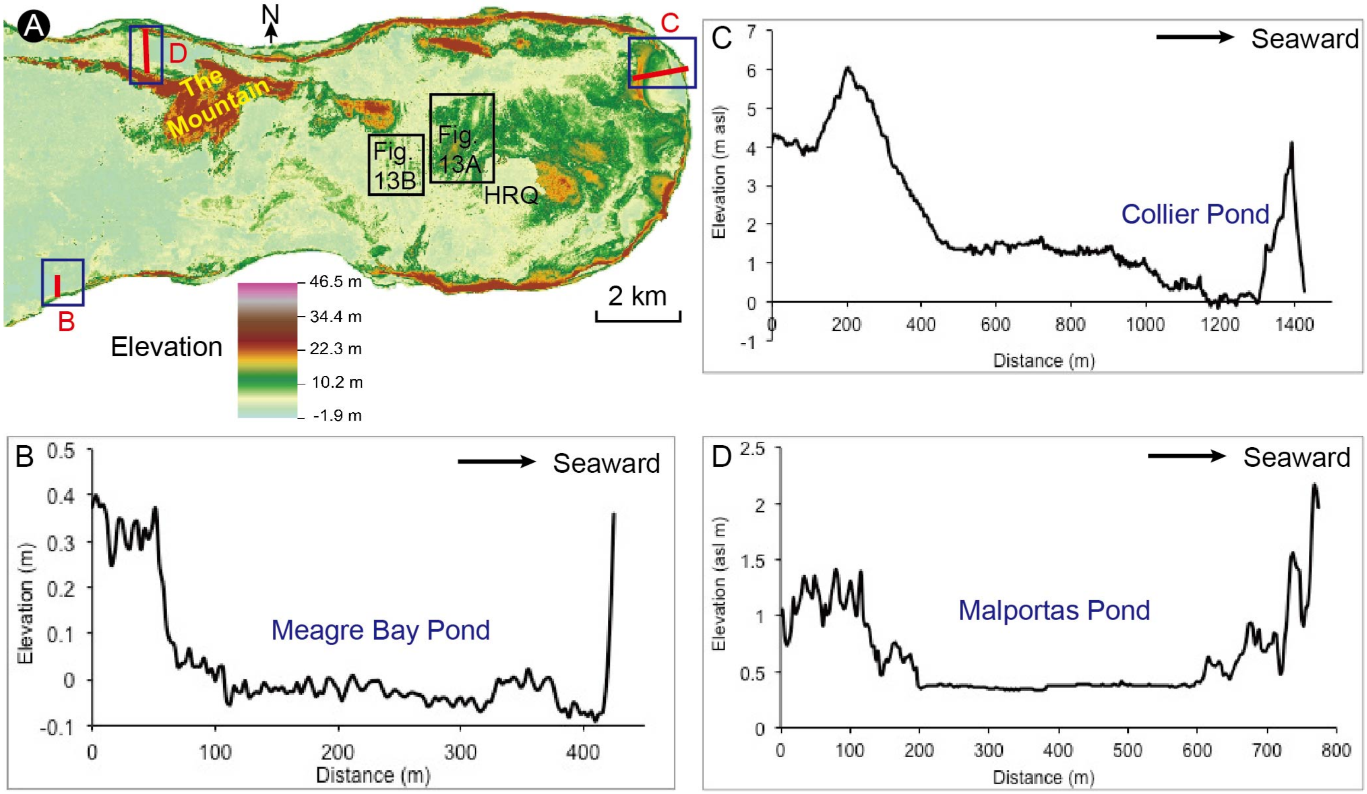
A
N
D
C
The Mountain
Fig. 13B
Fig. 13A
HRQ
B
2 km
Elevation
46.5 m
34.4 m
22.3 m
10.2 m
-1.9 m
C
Seaward
Collier Pond
Elevation (m asl)
Distance (m)
B
Seaward
Meagre Bay Pond
Elevation (m)
Distance (m)
D
Seaward
Malportas Pond
Elevation (asl m)
Distance (m)

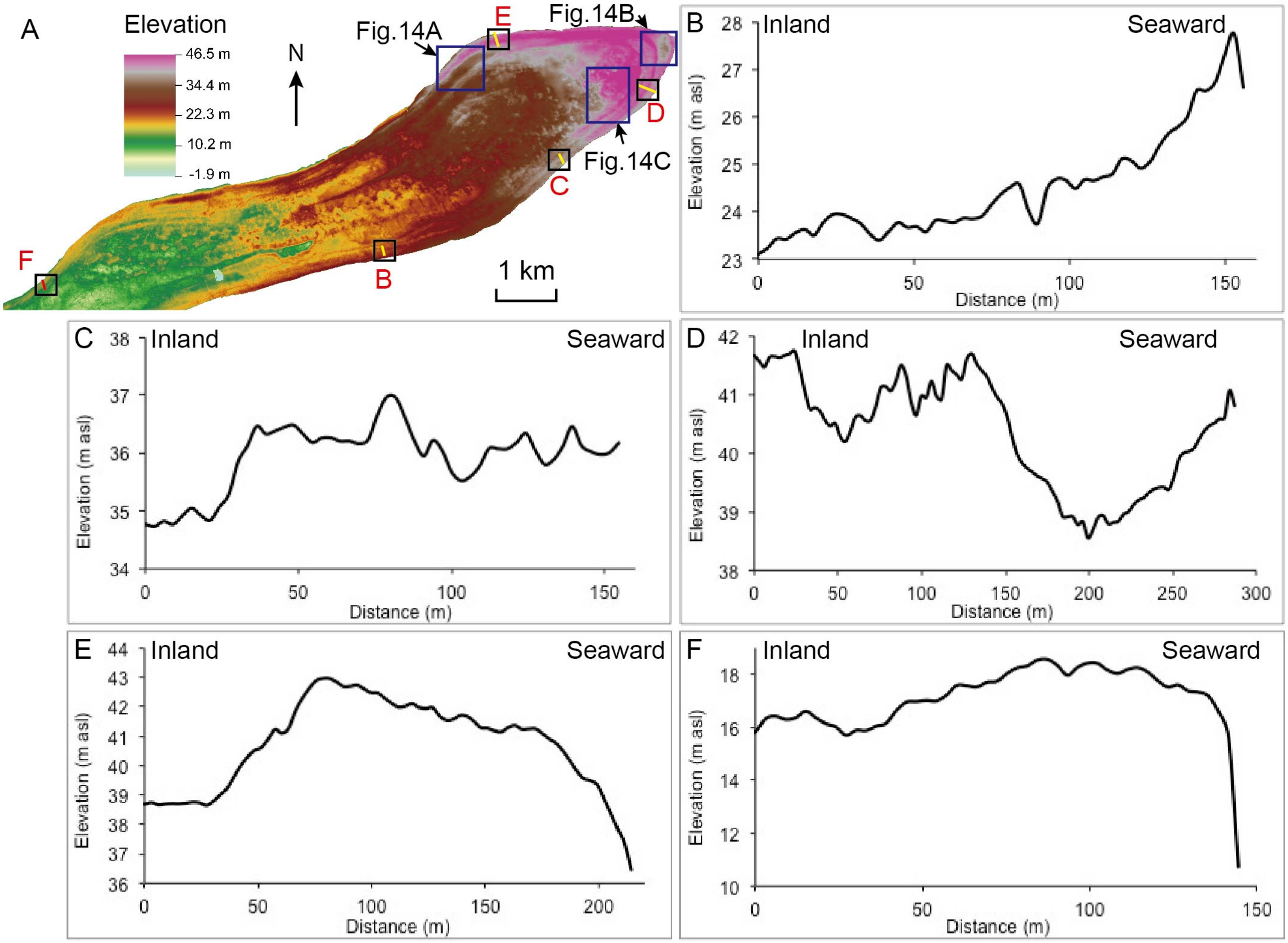
A
Elevation
46.5 m
34.4 m
22.3 m
10.2 m
-1.9 m
N
Fig.14A
E
Fig.14B
D
Fig.14C
C
F
B
1 km
B
Inland
Seaward
Elevation (m asl)
Distance (m)
C
Inland
Seaward
Elevation (m asl)
Distance (m)
D
Inland
Seaward
Elevation (m asl)
Distance (m)
E
Inland
Seaward
Elevation (m asl)
Distance (m)
F
Inland
Seaward
Elevation (m asl)
Distance (m)


A
B
C
D

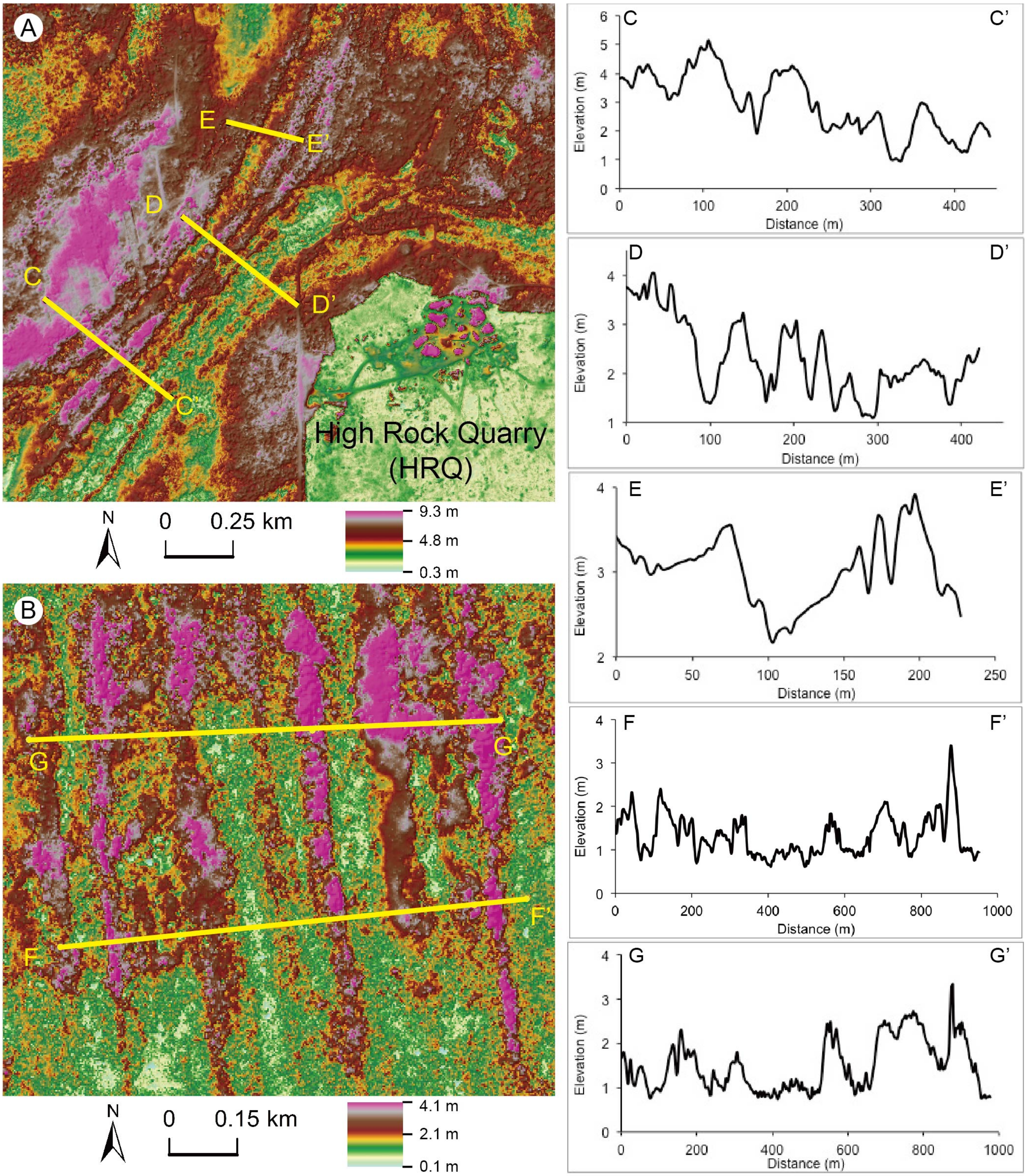

A
E
E'
D
C
D'
C'
High Rock Quarry
(HRQ)
N
0 0.25 km
9.3 m
4.8 m
0.3 m
B
G
G'
F
F'
N
0 0.15 km
4.1 m
2.1 m
0.1 m
C
C'
D
D'
E
E'
F
F'
G
G'
Elevation (m)
Distance (m)

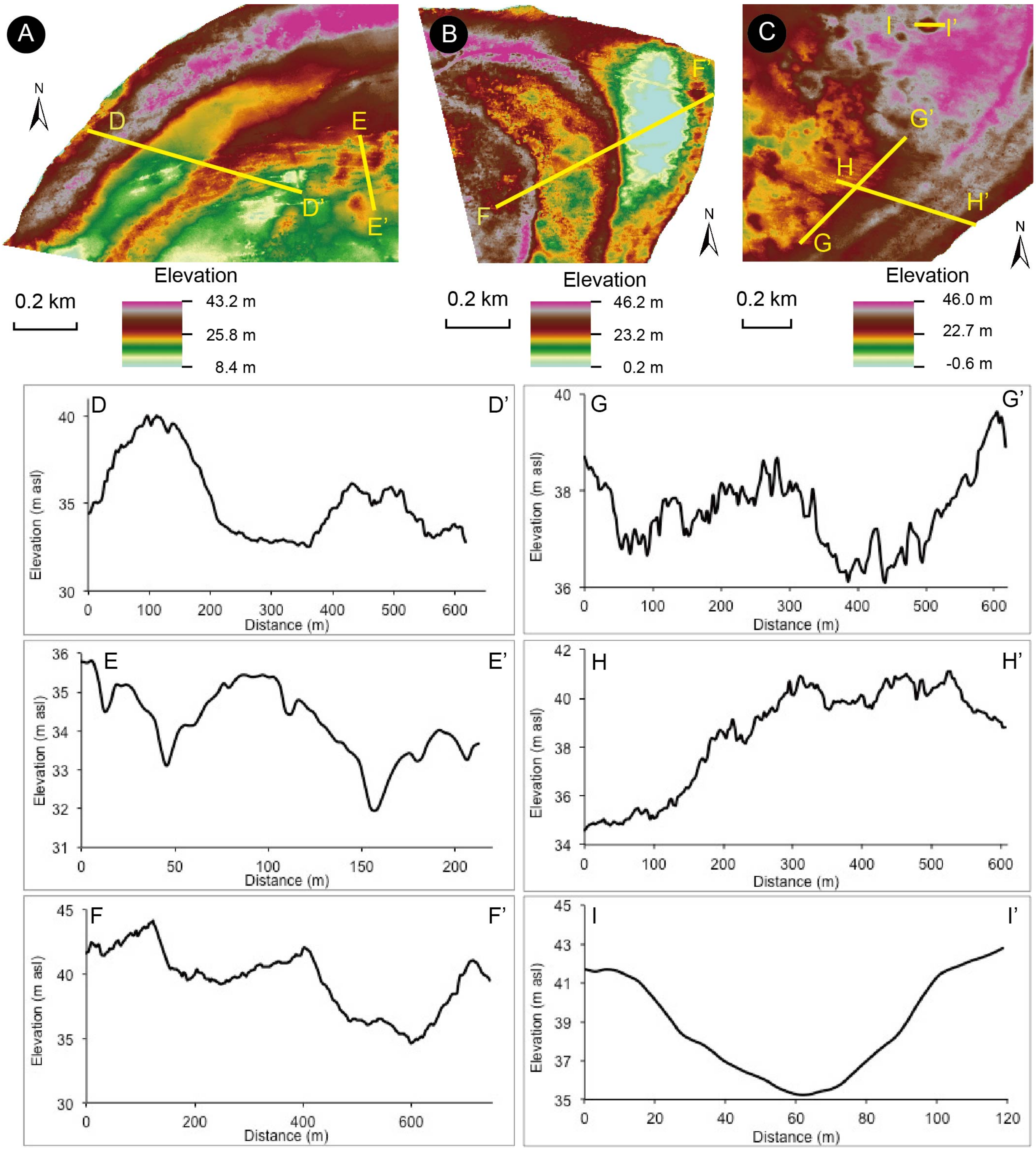
A
B
C
N
D
D'
E
E'
F
F'
G
G'
H
H'
I
I'
Elevation
0.2 km
43.2 m
25.8 m
8.4 m
46.2 m
23.2 m
0.2 m
46.0 m
22.7 m
-0.6 m
Elevation (m asl)
Distance (m)

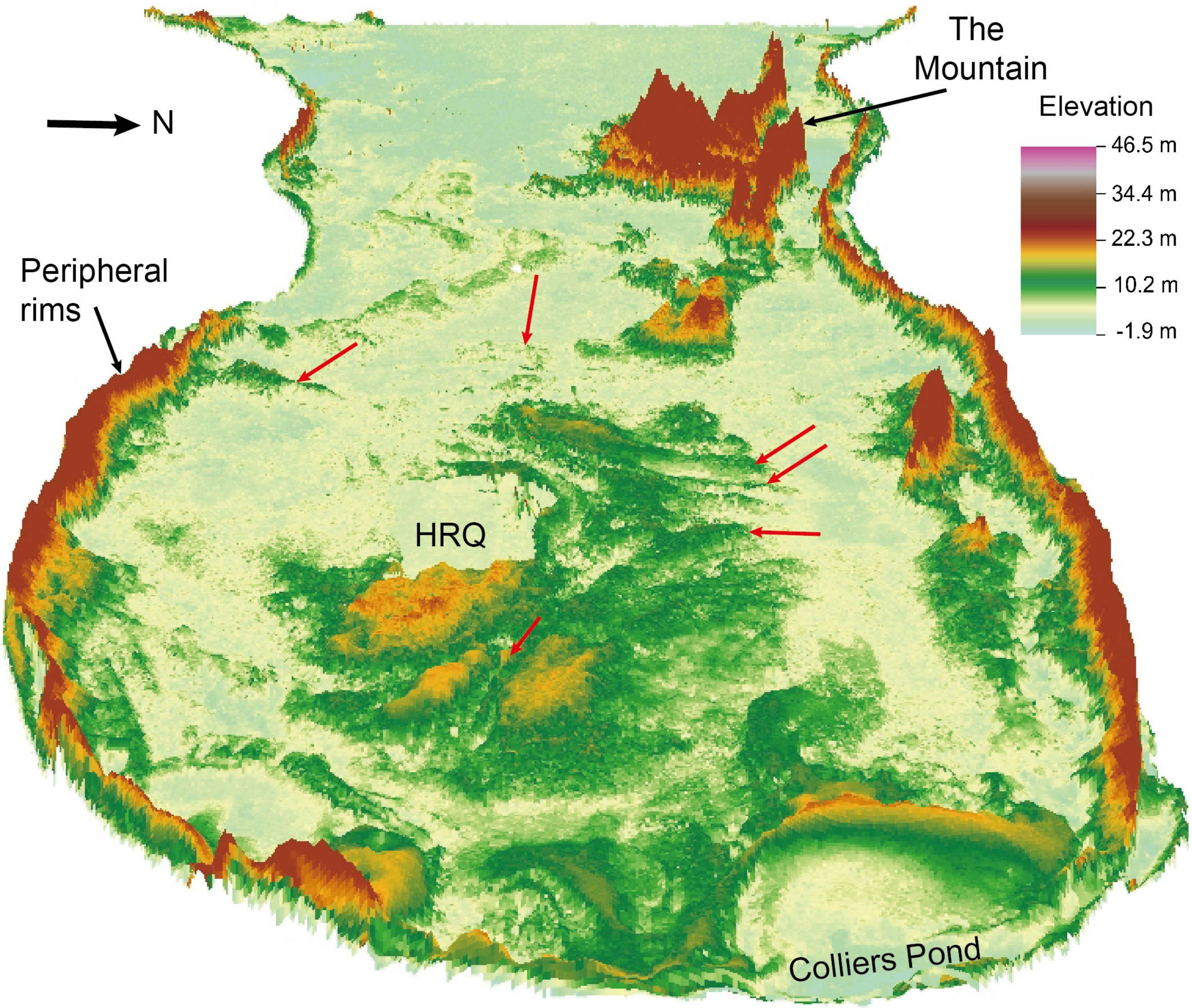

The Mountain
N
Elevation
46.5 m
34.4 m
22.3 m
10.2 m
-1.9 m
Peripheral rims
HRQ
Colliers Pond

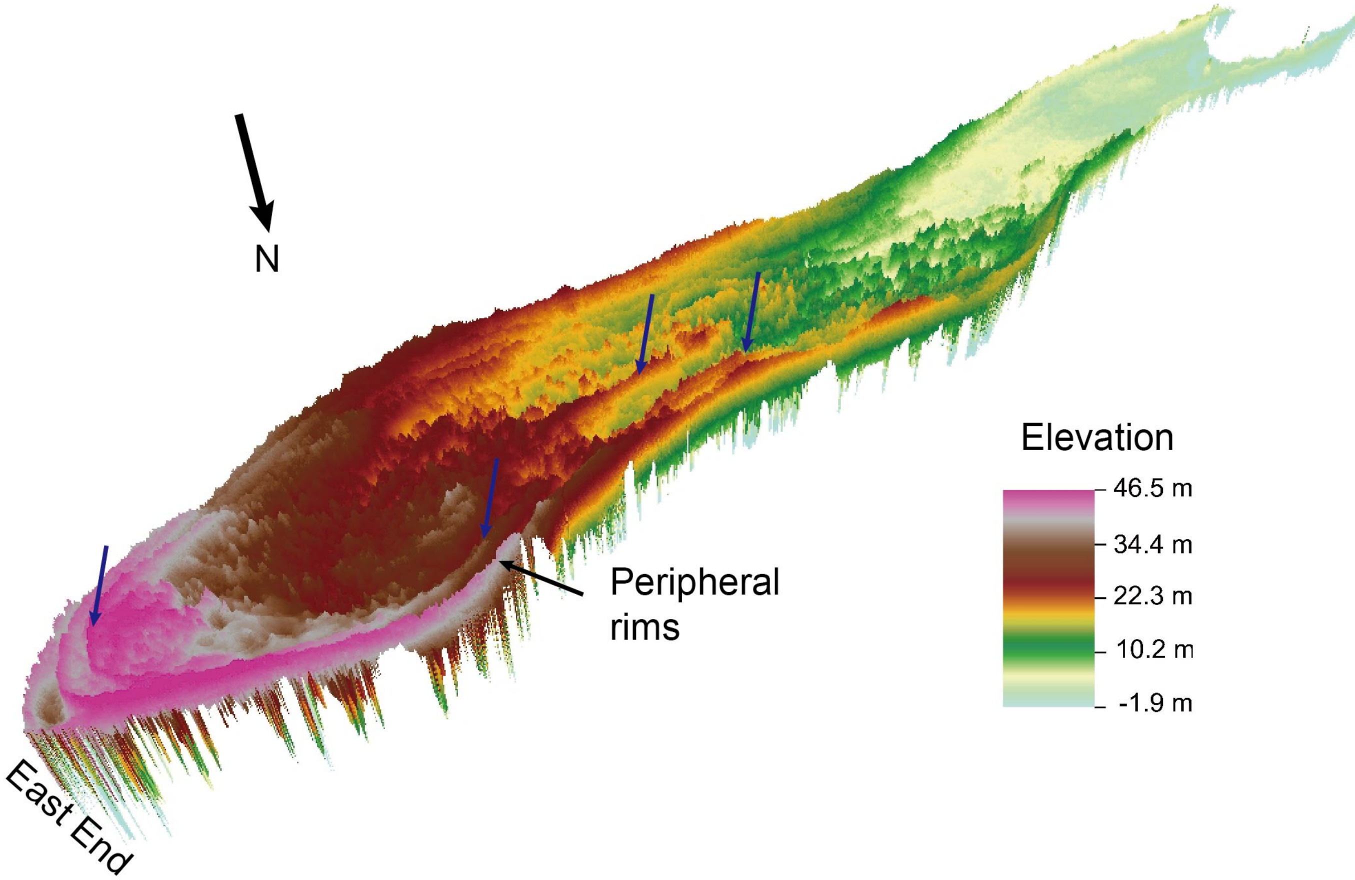
N
Elevation
46.5 m
34.4 m
22.3 m
10.2 m
-1.9 m
Peripheral rims
East End